

A Newtonian analogue of Kerr black hole

Areti Eleni *

Section of Astrophysics, Astronomy, and Mechanics, Department of Physics,
University of Athens, Panepistimiopolis Zografos GR15783, Athens, Greece

Theocharis A. Apostolatos †

Section of Astrophysics, Astronomy, and Mechanics, Department of Physics,
University of Athens, Panepistimiopolis Zografos GR15783, Athens, Greece

December 12, 2019

Abstract

A 250-year old Newtonian problem, first studied by Euler, turns out to share a lot of similarities with the most extreme astrophysical relativistic object, the Kerr black hole. Although the framework behind the two fields is completely different, both problems are related to gravitational fields that have quite intriguing analogies with respect to orbital motions of a test-body in them. The fundamental reason responsible for their extraordinary similarity is the integrability of both problems, as well as their common multipolar structure. In this paper we demonstrate the existence of a multitude of either qualitative, and sometimes quantitative, similarities between the two problems. Based on this analogy, one could use the Newtonian problem to get insight in cases where the relativistic treatment of the field of a Kerr black hole becomes quite complicated.

*email: aeleni@phys.uoa.gr

†email: thapostol@phys.uoa.gr

1 Introduction

Struggling to solve the three-body problem in Newtonian gravity, Euler studied in 1760 an easier version of the general problem: the problem of motion of a particle in the gravitational field of two fixed centers with masses m_1 , m_2 at a distance $2a$ apart from each other [1]. This problem, as it was much later shown by Whittaker [2], is characterized by such an internal dynamical symmetry that leads to a new integral of motion (according to Noether's theorem for mechanical particle systems), rendering this particular mechanical problem fully integrable.

On the other hand Kerr black holes, that were first described and studied by Kerr [3] as an exact solution of the vacuum equations of Einstein, proved to be the simplest macroscopic objects that Nature herself can create. They are fully described by only two parameters (the mass and the spin of the black hole, if we assume that the net electric charge of astrophysical objects is negligible according to astrophysical consensus); this is actually the physical context of the no-hair theorem [4]. During the golden era of general relativity (1970-1980) the physical characteristics of Kerr black holes, including perturbations of this metric, were studied extensively [5], and there is still an ongoing research on the subject in the framework of gravitational waves emitted from compact binaries [6], that is binaries consisting of neutron stars and/or black holes.

At least for binaries consisting of a massive rotating black hole and a neutron star, or a less massive black hole (known as extreme mass-ratio inspirals: EMRIs), could be studied perturbatively by considering geodesic orbits of the less massive counterpart in the gravitational field of a Kerr black hole [7]. The geodesic orbits around a Kerr black hole are described by an integrable system of differential equations (exactly as with the Newtonian gravitational field of the Euler problem), due to a Killing tensor field of the particular space-time that leads to a new integral of motion, the so called Carter constant [8, 9].

One might think that the similarity between the Euler problem and the Kerr metric ends exactly at this point, since the two gravitational fields do not look very similar from a physical point of view: Apart of the fundamental differences between the two corresponding physical frameworks (relativistic versus Newtonian gravity), the Kerr black hole describes an oblate gravitational field (due to its spin related to its axis of symmetry) of pure vacuum, while the Euler problem is by construction 'prolate' in the sense that the mass

of the system is distributed along its symmetry axis. However by introducing a purely imaginary distance –instead of a real one– between the two masses of the Euler problem [10], the corresponding gravitational potential remains real (the only necessary additional condition to obtain a real potential then is that the two masses m_1, m_2 are equal), while the global multipolar structure of its potential field becomes oblate; thus it becomes analogous to the Kerr gravitational field. Moreover, as Will [11] has shown, the only axisymmetrical and reflection symmetric Newtonian gravitational potential that leads to a third integral of motion that is quadratic in momenta (like the Carter constant) is the one that follows the same relation between successive multipole mass-moments with that of Kerr. Oddly enough, the Newtonian multipole mass-moments of the Euler problem with an imaginary distance are exactly the same with the Geroch-Hansen relativistic multipole mass-moments of the Kerr metric itself (the prolate version of the Euler field has the same ratio of moments but not the same moments). This very similarity between the two problems is fundamental for all the similarities of the orbital characteristics arising in both gravitational fields.

In this paper we have studied thoroughly the fundamental frequencies of the Eulerian orbits and have found numerous analogies with the frequencies of bound orbits in Kerr. Apart of the similarities in the expressions for the frequencies themselves, both problems have ISCOs. Moreover, one could find pairs of orbits –in both problems– that are characterized by exactly the same triplet of frequencies.

Stimulated by all these aforementioned analogies between the two problems, we have performed an extensive comparison of properties between the two problems and we found some new intricate similarities, that further persuaded us that the two problems could be considered quite faithful analogues of each other in Newtonian and relativistic frameworks, respectively. We believe that one could use this analogy to gain deeper insight into each one of them by studying its twin counterpart. As an example we have applied this analogy to clarify and explain the rather subtle argument of Kennefick and Ori [12] according to which the “circular” geodesic orbits in a Kerr background remain circular under their adiabatic evolution due to gravitational radiation. Not only the corresponding orbits in the Euler problem have analogous characteristics (they sweep over a surface of constant spheroidal radius that evolves adiabatically under a weak dissipative force), but the formulation of the Newtonian problem itself allows for a much more translucent explanation than the one used by Kennefick and Ori for first time. The Newtonian

variation of this proposition helps to better understand the foundations of that old but quite strong argument, and to explore it quantitatively in further detail.

Furthermore, the integrability of Kerr metric has been used in [13] to show that a hypothetical non-Kerr object could in principle be recognizable by its characteristic gravitational wave signal, due to its non-integrable character. During the crossing of an orbit in phase space through a Birkhoff island (the existence of which is a direct theoretical consequence of a slightly perturbed integrable system according to KAM theorem [14] and Poincaré-Birkhoff theorem [15]), the ratio of the corresponding frequencies in the signal spectrum should remain locked to a constant rational value for a while; this is the plateau effect which was analyzed in [13]. The initial computation of the relevant delay time was based on the average energy loss and average angular momentum loss as computed for a generic orbit in Kerr, suitably adjusted to account for the deviated lower multipole moments of the new space-time compared to the corresponding Kerr metric. In a foregoing paper, we plan to use the analogy between the Newtonian and the relativistic problem to check if this time interval could be systematically different if the evolution is computed by means of the instantaneous self-force acting on the particle, instead of being based on averaging formulae. The Newtonian problem could be easily perturbed to construct a slightly non-integrable system as a toy-model for a perturbed Kerr black hole.

The rest of the article is organized as follows: In Section 2 an overall description of the Euler problem is given, along with its oblate variant with an imaginary, instead of a real, distance. General characteristics of the orbits in the oblate Euler gravitational field is presented in Section 3. In Section 4 a list of the properties of the Euler problem, that are similar to the properties of Kerr metric, that are known up to now, are presented. In Section 5, an extensive list of new properties that reveal the close analogy between the two problems is presented. Finally, in Section 6, the argument of Kennefick and Ori from the perspective of the Euler problem is reformulated and explained. Furthermore, a quantitative result with respect to the evolution of the eccentricity of an orbit when the resonance condition is met –which actually could happen in ‘circular’ orbits in the Euler problem– is constructed. In Section 7 we summarize our findings, and suggest new problems that the similarity between Kerr and Euler field could further be used.

2 The Euler problem

2.1 The original problem

The gravitational field of two point-like (or spherically distributed) masses located at fixed positions in an inertial (in the Newtonian sense) frame of reference constitute the basis of the Euler problem, also known as the ‘*two-centre problem*’. Euler first studied the orbit of a test particle in such a gravitational field as an attempt to obtain analytical solutions in special cases of the general three-body problem (the motion of three particles of arbitrary masses under their mutual gravitational attraction). The gravitational potential of such a system is

$$V^{(E)}(r_1, r_2) = -\frac{Gm_1}{r_1} - \frac{Gm_2}{r_2}, \quad (1)$$

where G is the gravitational constant, m_1, m_2 are the two point-like masses and r_1, r_2 are the distances of the point, where the potential is computed, from the two fixed masses. If we use a coordinate system such that the two masses lie on the z -axis at equal distance a from the origin, then the gravitational field assumes the following form

$$V^{(E)}(\mathbf{r}) = -\frac{Gm_1}{|\mathbf{r} - a\hat{\mathbf{z}}|} - \frac{Gm_2}{|\mathbf{r} + a\hat{\mathbf{z}}|}. \quad (2)$$

This potential is obviously conservative and axially symmetric; consequently a test body orbiting this gravitational field will be described by a constant energy and a constant z -component of angular momentum. The potential is not reflection-symmetric about the $x - y$ plane, except when the two masses are equal. However, whatever the masses are, the problem is characterized by a hidden dynamical symmetry that leads to an unexpected new integral of motion, quadratic in momenta. This integral of motion –initially we shall call it ‘Euler’s third integral’– is derived by applying the Hamilton-Jacobi method when we perform separation of variables in a suitable coordinate system [16]. Although, this 3rd integral of motion is known for more than a century, quite recently, Lynden-Bell [17], trying to explain its physical meaning, offered a simple and straightforward constructive method to build it. He proved that its kinetic part is the scalar product of the angular momenta about the two centers of mass and defined it as:

$$I_3 = \frac{1}{2}(\mathbf{r}_1 \times \mathbf{v}) \cdot (\mathbf{r}_2 \times \mathbf{v}) - Ga\hat{\mathbf{z}} \cdot (m_1\hat{\mathbf{r}}_1 - m_2\hat{\mathbf{r}}_2), \quad (3)$$

where \mathbf{v} is the particle's velocity, $\mathbf{r}_{1,2} = \mathbf{r} \mp a\hat{\mathbf{z}}$ are the vectors from either gravitating mass to the test particle, while $\hat{\mathbf{r}}_{1,2}$ are the unit vectors along the directions of $\mathbf{r}_{1,2}$, respectively. I_3 does not depend on the mass of the test particle orbiting the corresponding field. The existence of three independent integrals of motion, render the motion in such a field describable by an integrable set of equations. Only a few known physics problems are exactly integrable, and all of them are characterized by special common properties (for example the motion in phase space lies on a 3-torus and each such torus is characterized by a triplet of fundamental frequencies).

A more appropriate coordinate system to study the motion in the Euler gravitational field is that of prolate spheroidal coordinates, where one of the two coordinates, ξ , is the sum of the distances from the two masses compared to the distance between the masses (this is the analogue of the radius of spherical coordinates, but endowed with an intrinsic length scale), while the other one, η , is the difference of the two distances divided again by the distance between the two fixed masses (this is the analogue of the cosine of the polar angle in spherical coordinates). The third coordinate is the usual azimuthal angle ϕ of spherical, or cylindrical coordinates. Thus

$$\xi = \frac{r_2 + r_1}{2a} = \frac{\sqrt{\rho^2 + (z+a)^2} + \sqrt{\rho^2 + (z-a)^2}}{2a}, \quad (4)$$

$$\eta = \frac{r_2 - r_1}{2a} = \frac{\sqrt{\rho^2 + (z+a)^2} - \sqrt{\rho^2 + (z-a)^2}}{2a}, \quad (5)$$

where ρ, z are the usual cylindrical coordinates. The spheroidal coordinates take values within the intervals: $\xi \in [1, +\infty)$ and $\eta \in [-1, 1]$. The inverse coordinate transformation yields

$$\rho = a\sqrt{(\xi^2 - 1)(1 - \eta^2)}, \quad (6)$$

$$z = a\xi\eta. \quad (7)$$

In terms of spheroidal coordinates (ξ, η) the Euler potential assumes the following form

$$V^{(E)}(\xi, \eta) = -G \frac{(m_1 + m_2)\xi + (m_1 - m_2)\eta}{a(\xi^2 - \eta^2)}. \quad (8)$$

The Lagrangian (per unit test-mass) of the Euler problem in spheroidal

coordinates is then:

$$L = \frac{1}{2}a^2 \left[(\xi^2 - \eta^2) \left(\frac{\dot{\xi}^2}{\xi^2 - 1} + \frac{\dot{\eta}^2}{1 - \eta^2} \right) + \dot{\phi}^2(\xi^2 - 1)(1 - \eta^2) \right] - V^{(E)}(\xi, \eta). \quad (9)$$

The corresponding canonical momenta in these coordinates are

$$p_\xi = a^2 \frac{\dot{\xi}}{\xi^2 - 1} (\xi^2 - \eta^2), \quad (10)$$

$$p_\eta = a^2 \frac{\dot{\eta}}{1 - \eta^2} (\xi^2 - \eta^2), \quad (11)$$

$$p_\phi = a^2 (\xi^2 - 1)(1 - \eta^2) \dot{\phi}. \quad (12)$$

and the Hamiltonian (per unit test-mass) assumes the following form

$$H = \frac{p_\xi^2}{2a^2} \frac{\xi^2 - 1}{\xi^2 - \eta^2} + \frac{p_\eta^2}{2a^2} \frac{1 - \eta^2}{\xi^2 - \eta^2} + \frac{p_\phi^2}{2a^2(\xi^2 - 1)(1 - \eta^2)} + V^{(E)}(\xi, \eta). \quad (13)$$

According to Landau's analysis [16] which is based on constructing the most general separable potential in such coordinates (called elliptical in Landau's textbook), the separability of the particular problem arises from the very fact that the numerator in equation (8) is a linear superposition of a function of ξ alone and a function of η alone. The integrability of this potential then arises as a direct consequence of the separability of Hamilton-Jacobi equation. The third conserved quantity, β in [16], besides the energy E and the z -angular momentum $L_z = p_z$, gets the following form in spheroidal coordinates:

$$\begin{aligned} \beta &= (\xi^2 - 1)p_\xi^2 + \frac{L_z^2}{\xi^2 - 1} - 2a^2(\xi^2 - 1)E \\ &\quad - 2G(m_1 + m_2)a\xi, \end{aligned} \quad (14)$$

$$\begin{aligned} &= -(1 - \eta^2)p_\eta^2 - \frac{L_z^2}{(1 - \eta^2)} + 2a^2(1 - \eta^2)E \\ &\quad + 2G(m_1 - m_2)a\eta. \end{aligned} \quad (15)$$

The two alternative expressions for β in Eqs. (14,15) are pure functions of p_ξ and ξ , or p_η and η , respectively, clearly demonstrating the separability of the problem. The constant β is related with the expression for I_3 of Eq. (3) by $\beta = -2I_3$, as one can verify by combining both expressions for β (Eqs. (14, 15)), expressed in cylindrical coordinates and performing a lengthy, but straightforward, computation.

2.2 The oblate version of the Euler problem

As mentioned in Section 1, the gravitational field of the Euler problem describes, by construction, a prolate distribution of mass as a source (this will become more obvious later on, in Sec. 4.2, when we will present the multipolar structure of the Newtonian problem). Therefore it does not resemble the gravitational field of a Kerr black hole, which is obviously oblate (its quadrupole moment is negative). However, it is easy to transform the original Euler problem into an oblate field by simply rotating a into a complex plane by $\pi/2$. Then a will transform into a purely imaginary distance, but the gravitational field will still be real, in the symmetric case where $m_1 = m_2 = M/2$. Only then the gravitational potential of each mass is given by the complex conjugate function of the potential of the other mass. In order to avoid confusion we will keep considering the a parameter real and simply replace a by ia in the potential. The corresponding gravitational field –henceforth called the oblate Euler field– assumes the following form:

$$V^{(oE)} = -\frac{G(M/2)}{|\mathbf{r} - ia\hat{\mathbf{z}}|} - \frac{G(M/2)}{|\mathbf{r} + ia\hat{\mathbf{z}}|} \quad (16)$$

where by $|\mathbf{k}|$ we mean $\sqrt{\mathbf{k} \cdot \mathbf{k}}$. The latter vector product is a complex number and in order to keep the square root single-valued we should adopt a branch cut. We have chosen the negative real axis of the vector product as the branch-cut of our potential function. After some algebra the new potential (from now on we will use only this potential, so we will simply write it V) takes the following form in usual spherical coordinates:

$$V(\mathbf{r}) = -\frac{GM}{\sqrt{2}} \frac{\sqrt{R^2 + r^2 - a^2}}{R^2}, \quad (17)$$

where

$$\begin{aligned} R^2 &= \sqrt{(r^2 - a^2)^2 + (2a\mathbf{r} \cdot \hat{\mathbf{z}})^2} \\ &= \sqrt{(r^2 - a^2)^2 + 4a^2r^2 \cos^2 \theta}. \end{aligned} \quad (18)$$

Although it is not obvious at this point that the new potential describes an actually oblate field, its true character will be unequivocally revealed in Section 4.2, where its multipole moments are written.

It should be noted that the new field $V(\mathbf{r})$ is defined everywhere since $R^2 \geq r^2 - a^2$, except of along the equatorial circle ($r = a, \theta = \pi/2$) where the potential becomes indeterminate, since then $R^2 = r^2 - a^2 = 0$. Also, on the equatorial disk ($r < a, \theta = \pi/2$) the potential vanishes. The oblate Euler field is reflection symmetric, as the original prolate Euler field when the masses of its two gravitational centers are equal.

A more appropriate coordinate system to study the motion in this oblate field is that of oblate spheroidal coordinates, (ξ, η, ϕ) , which are defined as:

$$x = a\sqrt{(1 + \xi^2)(1 - \eta^2)} \cos \phi, \quad (19)$$

$$y = a\sqrt{(1 + \xi^2)(1 - \eta^2)} \sin \phi, \quad (20)$$

$$z = a\xi\eta, \quad (21)$$

where $\xi \in [0, +\infty)$, $\eta \in [-1, 1]$ and $\phi \in [0, 2\pi)$. The surfaces of constant ξ -coordinate are oblate ellipsoids of revolution with focal circle ($r = a, \theta = \pi/2$), while the surfaces of constant η -coordinate are one-sheet half hyperboloids of revolution sharing the same focal circle with the above ellipsoids.

In terms of oblate spheroidal coordinates the Euler potential assumes the following simple form

$$V(\xi, \eta) = -\frac{GM\xi}{a(\xi^2 + \eta^2)}. \quad (22)$$

The Lagrangian (per unit test-particle mass) of the oblate Euler potential becomes:

$$L = \frac{1}{2}a^2 \left[(\xi^2 + \eta^2) \left(\frac{\dot{\xi}^2}{\xi^2 + 1} + \frac{\dot{\eta}^2}{1 - \eta^2} \right) + \dot{\phi}^2(\xi^2 + 1)(1 - \eta^2) \right] - V(\xi, \eta), \quad (23)$$

while the corresponding Hamiltonian is

$$H = \frac{1}{2a^2} \left[p_\xi^2 \frac{\xi^2 + 1}{\xi^2 + \eta^2} + p_\eta^2 \frac{1 - \eta^2}{\xi^2 + \eta^2} + \frac{p_\phi^2}{(\xi^2 + 1)(1 - \eta^2)} \right] + V(\xi, \eta), \quad (24)$$

with the canonical momenta defined as:

$$p_\xi = a^2 \frac{\xi^2 + \eta^2}{\xi^2 + 1} \dot{\xi} \quad (25)$$

$$p_\eta = a^2 \frac{\xi^2 + \eta^2}{1 - \eta^2} \dot{\eta} \quad (26)$$

$$p_\phi = a^2(\xi^2 + 1)(1 - \eta^2)\dot{\phi}. \quad (27)$$

Repeating Landau's argument [16], for the oblate field now, the very fact that the numerator in Eq. (22) is again a linear superposition of a function of ξ and a function of η (no presence of η function here) lies behind the separability of the given problem, and consequently, the integrability of this particular potential. The third conserved quantity, β , besides the energy E and the z -angular momentum $L_z = p_\phi$, takes the following form:

$$\beta = -(1 - \eta^2)p_\eta^2 - \frac{L_z^2}{(1 - \eta^2)} - 2a^2E(1 - \eta^2) \quad (28)$$

$$= (\xi^2 + 1)p_\xi^2 - \frac{L_z^2}{(\xi^2 + 1)} - 2a^2E(\xi^2 + 1) - 2GMa\xi. \quad (29)$$

Once again, the separability of the problem is clearly manifested in these two expressions since the 4D phase space of ξ, p_ξ, η, p_η breaks in two independent 2D phase spaces ξ, p_ξ and η, p_η , and the motion evolves along a closed line in each of these two phase planes.

3 The orbital characteristics in oblate Euler

The gravitational potential of the Euler problem (henceforth we will only deal with the oblate version of the Euler problem and we will omit any specific notation mark) describes a conservative axisymmetric field that admits a constant of motion, as we have mentioned earlier, that is quadratic with respect to momenta. This new constant could be considered as an analogue of the square of angular momentum of central fields. The new field is by construction not central though, but its dynamical structure is such that it renders the problem integrable. Furthermore, the choice of imaginary distance between the two masses renders the field oblate with respect to its dynamics, instead of prolate. This very fact make it more physical with respect to qualitative resemblance with spinning astrophysical objects.

The Kerr metric is a relativistic object of extreme astrophysical interest, which shares a lot of general properties with the Euler field as it will

be shown in the following Sections of the article. Both gravitational fields are (i) integrable (with respect to the description of geodesic orbits of test particles orbiting around them), characterized by three, similar in context, constants of motion, (ii) have similar multipolar characteristics, and (iii) are fully described by only two physical parameters, their total mass and the spin parameter (for the Kerr) or the imaginary part of the distance between the two masses (for the Euler).

In the following section we will further study the orbital characteristics of the Euler problem in order to demonstrate the extent of similarity between the two fields.

3.1 Equations of motion

In order to compare the equations of motion in the Euler potential with those of Kerr we define new coordinates:

$$r = a\xi, \quad (30)$$

$$\theta = \cos^{-1} \eta. \quad (31)$$

The new (r, θ) coordinates play the role of the radial and the longitudinal Boyer-Lindquist (BL) coordinates of Kerr space-time, respectively. Although equivalent to the oblate spheroidal coordinates ξ, η , the new coordinates r, θ are better suited to reveal the analogies with the corresponding orbits of Kerr metric. The 3rd coordinate, ϕ , is the usual azimuthal angle that is common in both problems. The comparison will be further simplified by adopting geometrized units ($G = c = 1$) in the Newtonian field as well.

The Euler potential in these new coordinates is given by:

$$V(r, \theta) = -\frac{Mr}{r^2 + a^2 \cos^2 \theta}, \quad (32)$$

while the corresponding Hamiltonian (24) yields the following form:

$$H = \frac{(r^2 + a^2)p_r^2 + p_\theta^2}{2\Sigma} + \frac{p_\phi^2}{2(r^2 + a^2) \sin^2 \theta} - \frac{Mr}{\Sigma}, \quad (33)$$

where $\Sigma = r^2 + a^2 \cos^2 \theta$, while p_r, p_θ, p_ϕ are the canonical momenta with respect to r, θ, ϕ , respectively. The momenta p_r and p_θ are related with the momenta p_ξ and p_η (c.f., Eqs. (25, 26)), respectively, through the following

relationships: $p_r = p_\xi/a$ and $p_\theta = -\sin\theta p_\eta$. Since ϕ coordinate is missing from the Hamiltonian, p_ϕ is conserved, and henceforth we will write it, instead, L_z .

Applying the Hamilton-Jacobi method in the above Hamiltonian (33), we obtain the following separated equations of motion for a test particle:

$$\Sigma \left(\frac{dr}{dt} \right) = \pm \sqrt{V_r(r)}, \quad (34)$$

$$\Sigma \left(\frac{d\theta}{dt} \right) = \pm \sqrt{V_\theta(\theta)}, \quad (35)$$

$$\frac{d\phi}{dt} = \frac{L_z}{(r^2 + a^2) \sin^2 \theta}. \quad (36)$$

The radial potential $V_r(r)$ and the longitudinal potential $V_\theta(\theta)$ introduced in Eqs. (34, 35) are given by:

$$V_r(r) = 2Er^4 + 2Mr^3 + (2a^2E - Q - L_z^2)r^2 + 2Ma^2r - Qa^2, \quad (37)$$

$$V_\theta(\theta) = Q - \cos^2 \theta \left(-2a^2E + \frac{L_z^2}{\sin^2 \theta} \right). \quad (38)$$

where E is the constant value of the Hamiltonian, L_z is the conserved z -component of its angular momentum and Q is a third integral of motion that naturally emerges from the above separation of variables, while t is the Newtonian time parameter. In the next section 3.2, we define all these constants of motion in detail.

At this point, it should be noted that exactly the same equations of motion, but with slightly different potentials V_r, V_θ , show up in the description of the geodesics in Kerr metric. However in Kerr case the proper time τ , instead of the coordinate time t , is the evolution parameter of the spatial BL coordinates r, θ, ϕ .

The Eulerian orbits are performing a radial oscillation and a precession while they revolve around the axis of symmetry. The characteristics of V_r are responsible for the radial oscillation, while those of V_θ are responsible for the oscillation of the test particle about the equatorial plane.

3.2 Bound orbits

As demonstrated in the previous section (c.f. Section 3.1), the Euler potential admits three constants of motion, which in terms of coordinates and momenta

are given by the following expressions:

$$E = \frac{p_r^2(r^2 + a^2) + p_\theta^2}{2\Sigma} + \frac{p_\phi^2}{2(r^2 + a^2)\sin^2\theta} - \frac{Mr}{\Sigma}, \quad (39)$$

$$L_z = p_\phi, \quad (40)$$

$$Q = p_\theta^2 + \cos^2\theta \left(-2Ea^2 + \frac{L_z^2}{\sin^2\theta} \right) \quad (41)$$

$$= -p_r^2(r^2 + a^2) + 2Er^2 + 2Mr - \frac{L_z r^2}{r^2 + a^2}. \quad (42)$$

The third integral of motion Q , written in two alternative forms in Eqs. (41, 42), one with respect to r, p_r , and one with respect to θ, p_θ , is related to Lynden-Bell's I_3 , and Landau's β , through the relation:

$$\beta = -2I_3 = -Q - L_z^2 - 2a^2E. \quad (43)$$

We have decided to use Q , instead of β and I_3 , as the third integral of motion, because this form of Q could be considered as the Newtonian analogue of Kerr's Carter constant, as it will be shown later.

The two potentials V_r, V_θ , presented in the previous section, share a lot of similarities with the corresponding potentials of Kerr. More specifically, the later one, V_θ , yields exactly the same form as V_θ of Kerr, if we simply replace E by $(E^2 - 1)/2$ (see Section 5.2), while V_r is of order four, like that of Kerr, and most of the polynomial coefficients coincide with those of Kerr, if the previous reparametrization of E is imposed here as well. Especially the fact that $V_r(r)$ is a quartic polynomial, leads to the possibility of two families of bound orbits: (a) one with lower radii: $0 \leq r_4 \leq r \leq r_3$, coexisting with another one with $r_3 \leq r_2 \leq r \leq r_1$, where r_1, r_2, r_3, r_4 are real roots of the polynomial V_r , and (b) one with only a single range of radii $r_2 \leq r \leq r_1$, while the other set of roots of V_r are then complex conjugate to each other. We will consider bound orbits that correspond to the farthest family, if two of those exist. The reason is the following: the bound geodesic orbits in Kerr are either those that remain at the exterior of the event horizon, or plunging orbits that eventually cross the black hole horizon. The former ones are the ones at higher values of radii far from the horizon.

The family of orbits in Euler corresponding to lower radii, when both families are present, will be considered 'plunging orbits' at close analogy to those of Kerr. The second type (b) of bound orbits in Euler, with a single

range of allowed radii, could either describe a normal bound orbit (without any plunging pair), or an effectively ‘plunging orbit’ in the sense that the two distinct regions of bound orbits of the first type have merged into a single region through a potential neck that will eventually drive an orbit to a plunging one (see Figure 1(d)). The latter type of orbits will not be treated as simple eccentric orbits with a periastron and an apastron, since it does not seem natural to describe them as orbits with a specific semi-latus rectum and eccentricity. In our description of possible bound orbits in the Euler potential we will not consider such type of orbits.

Next we will follow the same procedure one uses to study the bound orbits of Kerr: we will parametrize the roots of $V_r(r)$ as follows

$$r_1 = \frac{p}{1-e} \quad , \quad r_2 = \frac{p}{1+e}, \quad (44)$$

assuming they correspond to the outer bound orbit (if there exists an inner region as well) described by the dimensional semi-latus rectum p and the eccentricity e . The rest of the roots of V_r , r_3, r_4 (either real or complex) could then be computed as functions of the orbital parameters p, e and the inclination angle of the orbit $\pi/2 - \theta_{\min}$ (where θ_{\min} is the lowest polar angle of the orbit). The set of the three orbital parameters (p, e, θ_{\min}) could be used not only to compute the roots of V_r , but from them one could compute the constants of motion, as well (see Appendix B).

Meanwhile, the oscillation of θ parameter around the equatorial plane ($\theta = \pi/2$) is governed by V_θ potential as mentioned previously. The roots of V_θ are two real supplementary angles which correspond to the turning points of orbital-plane oscillation and two complex imaginary angles. The roots of V_θ are described in Appendix B.

As mentioned above, the constants of motion E , L_z and Q are directly related to the orbital parameters p, e, θ_{\min} , but they are not as easy to handle as the orbital parameters. Although analytic expressions for p, e, θ_{\min} as functions of E, L_z, Q could be written they are quite involved. Furthermore, by fixing the constants of motion, one could get a set of two bound orbits, an interior one and an exterior one, but then one has to choose to which one a semi-latus rectum and an eccentricity should be assigned. In contrast, as long as one gets restricted in a meaningful space of p, e, θ_{\min} the orbit is unambiguously determined. This is actually the reason we have chosen to use the orbital parameters in order to parametrize the orbits.

3.3 The separatrix

In the 3-dimensional space of orbital parameters (p, e, θ_{\min}) there is a special surface, which corresponds to a pair of orbits: one normal bound orbit and a “plunging” one that share a common turning point, that is $r_2 = r_3$ (c.f. Figure 1(b)). This surface is the separatrix. The normal bound orbits of the separatrix are actually marginally stable orbits. Eventually these orbits will evolve into circular orbits with radius $r(t \rightarrow \infty) = r_2 = r_3$. One expects that a slight variation of the physical parameters of the orbit (E, L_z, Q) , due to any kind of dissipative self-force acting on the test particle, could cause the two families of orbits to either communicate (by transforming the normal bound orbits into “effectively plunging” orbits), or move the two types of orbits further apart. Actually, the neighborhood of mostly the whole surface of the separatrix corresponds to the latter case. Both sides of the surface (but close to it) describe pairs of two distinct separated families of orbits, one above the separatrix with orbital parameters $(p_1, e_1, \theta_{\min})$ and one below the separatrix with orbital parameters $(p_2, e_2, \theta_{\min})$ with $p_1 > p_s > p_2$, such that both are described by the same V_r potential with the same constants of motion. The one with p_2 is actually the plunging one, dual to the normal one with p_1 ; therefore we will deal only with orbits located ‘above’ the separatrix.

Near the edge of the separatrix (corresponding to the most inclined orbits of the separatrix) there are orbits that are effectively plunging ones like that of Figure 1(d) and as we mentioned earlier, we will not study such orbits.

The separatrix could be described as follows: For a given pair of eccentricity, e , and inclination, $\pi/2 - \theta_{\min}$, there is a specific semi-latus rectum $p_s(e, \theta_{\min})$ that brings the two types of orbits (the exterior normal orbit and the interior plunging one) in touch. For equatorial orbits, $\theta_{\min} = \pi/2$, one could easily obtain an analytic expression for $p_s(e, \theta_{\min} = \pi/2)$ (by setting $Q = r_4 = 0$ and, $r_3 = r_2 = p/(1 + e)$, while $r_1 = p/(1 - e)$ in Eq. (37), and write it in terms of the roots of the polynomial). For generic inclined orbits though it is a bit more difficult to obtain an analytic expression for p_s as a function of e , and θ_{\min} . We found useful to introduce an additional parameter $x := r_4/r_3$, in order to write an analytic expression for $p_s(e, x)$ and then plot the surface $p_s(e, \theta_{\min})$ in parametric form, since θ_{\min} itself could be directly expressed as a function of e, x as well. In Figure 3.3 the separatrix surface has been plotted for a specific value of a , namely $a = 0.5M$. All the above analytic derivations are thoroughly analyzed in Appendix C.

The separatrix extends from $\theta_{\min} = \pi/2$ (equatorial orbits) to a minimum

value of θ_{\min} that depends –not very sensitively– on the eccentricity, e . More specifically $\theta_{\min} \simeq 65.5^\circ$, for $e = 0$, and it increases monotonically to $\theta_{\min} \simeq 70.5^\circ$, for $e = 1$. The overall shape of the surface is the same for any value of a , while the value of p_s scales linearly with a , assuming its highest value, $p_{s,\max} = 2a/M$, for $e = 1$, $x = 0$ (which corresponds to $\theta_{\min} = \pi/2$). Beyond the lower θ_{\min} values there is no separatrix; that is, there are no more four real roots of V_r . A complex pair of roots arise then.

Now let us study in further detail the region of parameter space outside the separatrix. On the region just above (but not far from) the separatrix ($p > p_s$) the two types of orbits (stable bound and “plunging”) get separated ($r_2 > r_3$). As we mentioned previously, below the separatrix the order of roots is alternated $r_2 < r_3$; therefore there is lack of physical description of such orbits based on the assumption that the order of roots is $r_1 \geq r_2 \geq r_3 \geq r_4$ and the bound orbit oscillates radially between r_1 and r_2 . Each such point (p, e, θ_{\min}) , located below the separatrix, has its dual above the separatrix with a different set p', e' –but with the same inclination– such that $r_1 = p/(1-e) = r'_1 = p'/(1-e') \geq r'_2 = p'/(1+e') = r_3 \geq r'_3 = r_2 = p/(1+e) \geq r'_4$, therefore both these points correspond to a normal bound orbit that oscillates radially between r'_1 and r'_2 . Far from the separatrix surface (either below or above it) the potential V_r looses a pair of real roots, thus, then, there is only a single bound orbit corresponding to it. Finally in a rather narrow space around the boundary of the separatrix, corresponding to the lower possible value of θ_{\min} , there is a bizarre type of bound orbits (the effectively plunging orbits) arising from the merging of a stable bound orbit with a “plunging” one. The potential in such cases has a local minimum between its two real roots (see Figure 1(d)). Although we will not deal with such orbits, there is a finite lower and a finite higher allowed radius for those as well, so one could still use the analytic expressions for the frequency of the radial oscillations, which we will introduce later on.

Especially the boundary of the separatrix with $e = 0$ corresponds to marginally stable “spherical” orbits (or, as they are usually called in Kerr metric, “circular” orbits). It should be noted that the boundary of the separatrix corresponding to equatorial orbits ($\theta_{\min} = \pi/2$) is given by a monotonically increasing function $p_s(e)$, like in Kerr, but it has the opposite sign of curvature. In both problems the “corner” of the separatrix at $e = 0$ and $\theta_{\min} = \pi/2$ (equatorial orbit), which corresponds to the ISCO, represents the lowest semi-latus rectum among all marginally stable spherical orbits.

4 Known analogies

In this section we present a list of the analogies between the two problems, the Euler and Kerr, that have already been shown in the literature by various authors in the past. Most of these analogies were presented in different context from the one followed in this article and in most of them there is no clear connection between Kerr and oblate Euler field.

4.1 Basic common characteristics and fundamental differences

During the golden era of black holes, when extensive mathematical studies had been performed, Israel [18] ended up in the oblate Euler field (without recognizing it as such) as the Newtonian analogue of Kerr metric by means of the right source distribution of the gravitational field. Actually the analogy between the two fields had been revealed even earlier by Keres [19], but it was mainly focused on finding similar properties related to the ring singularity of the then recently discovered Kerr metric and the corresponding avoidance of the ring singularity by geodesics. There was no demonstration of any connection between the two gravitational fields with respect to the orbital characteristics in them.

The present study attempts to extend this old found similarity between the two fields, mostly in the direction of astrophysically oriented issues, like geodesic orbits at the exterior of a Kerr black hole and their properties.

It should be pointed out though, that there are fundamental differences between the two fields. At first glance there is a dimensional difference of the parameter a showing up in the two fields. For the Kerr metric the a parameter is related to the spin of the Kerr black hole, thus it has dimensions of length times velocity (it is actually the ratio of the angular momentum of the black hole to its mass $a = S/M$). In Euler's oblate problem the a parameter is simply a length. Although in geometrized units, both a parameters have length dimensions, (or equivalently mass dimensions) the two a 's still have completely different physical origin. Despite that, this parameter, (or its dimensionless counterpart $a_\star = a/M$ in geometrized units where $G = c = 1$), seems to play the same role as an adjusting parameter of the two fields and their correspondence.

However there is an essential difference in the use of a in the two problems: in Euler's problem a_\star could assume any value, while in Kerr a_\star cannot exceed

the value of 1 (hyperextreme Kerr). However the restriction for the a_* in Kerr is mainly related to the existence of a horizon in Kerr, which has no analogue in Newtonian gravity in the first place. Here we will restrict our study of the Euler field in the range $a_* \in (0, 1]$.

Another technical difference arising between the two problems is the asymmetry of Kerr metric under the transformation $\phi \rightarrow -\phi$ (one should amend such a transformation with $t \rightarrow -t$, as well, to produce an isometry, but then the Kerr spin parameter a will change its sign). By contrast, Euler's problem (as any other type of axisymmetric Newtonian potential) is completely symmetric under such a transformation $\phi \rightarrow -\phi$. Consequently, the dragging of frames arising in stationary axisymmetric relativistic configurations, like in Kerr, does not have its analogue in Newtonian gravity. Therefore we shall be very careful when we compare the quantitative characteristics of phenomena that are sensitive to the sense of rotation in Kerr, with the corresponding ones in Euler's field.

4.2 Multipolar structure

More recently, Will [11] showed that the Newtonian axisymmetric gravitational field that is characterized by a third conserved quantity analogous to the Carter constant of a Kerr space-time (that is quadratic in momenta), leading, consequently, to an integrable Newtonian potential, should have a multipolar expansion that follows exactly the same relation as the mass multiple moments M_{2l} of the Kerr metric itself, that is

$$M_{2l} = M \left(\frac{M_2}{M} \right)^l, \quad (45)$$

while its odd- l mass moments vanish (as one would expect for a reflection symmetric gravitational field). It should be noted that this multipolar structure describes exactly the Euler's field (both the oblate and the prolate one) with equal masses. More specifically, if $M_2 > 0$ it corresponds to the original Euler's field (the prolate one), while if $M_2 < 0$ it corresponds to the oblate version of the Euler's field. Naturally, the case $M_2 = 0$ is the monopole, spherically symmetric, Keplerian field, for which the corresponding third integral of motion is simply the square of the total angular momentum of an orbiting test particle, instead of the constant Q , discussed in the previous section.

Of course a Newtonian stationary and axisymmetric potential cannot reproduce any effect like the dragging of frames of the corresponding relativistic field, and thus there are no current-mass multipole moments like that of Kerr. This is one of the basic differences between the two fields, and that renders the comparison between the corresponding orbits in the two fields more subtle. We will further discuss this subtlety in Section 5.3.

Later on Markakis [20] attempted to generalize Will's result, looking for Newtonian gravitational fields that admit integrals of motion of higher order (in particular quartic with respect to momenta). His analysis yielded a null result. If the analogy between the Euler's problem and the Kerr metric could be extended to problems with other type of non-Carter-like integrals of motion, the negative result of Markakis could be just a hint that probably there is no integrable vacuum stationary and axisymmetric solution describing an isolated object other than the Kerr in General Relativity.

4.3 The separability of the wave equation

As it was shown in [21] the gravitational field of the Euler's problem, not only leads to a lot of similarities in the characteristics of test-particle orbits with those of the gravitational field of Kerr, but the separability arising in the equations that determine the orbits (for both problems), is also exhibited in the scalar wave equation in both gravitational fields. Therefore the Newtonian type of wave equation

$$\square\Psi = -\kappa V\Psi, \quad (46)$$

where V is a Newtonian potential, and κ is a constant with dimensions of frequency squared, becomes separable in spheroidal coordinates if the potential is that of the Euler's problem. Moreover, the wave solutions of the oblate Euler's problem can be written as a product of an angular part that has exactly the same form as the corresponding angular part of the scalar perturbations in Kerr, while the radial part has qualitatively very similar behavior, especially if $\kappa = 4\omega^2$, where ω is the corresponding frequency of the wave solution. To reveal this magnificent analogy one should consider the following correspondence:

$$\eta^{(\text{Euler})} \leftrightarrow \cos\theta^{(\text{Kerr})}, \quad (47)$$

$$r^{(\text{Euler})} = a\xi^{(\text{Euler})} \leftrightarrow \tan\left(a\int_{r_{\min}^{(\text{Kerr})}}^{r^{(\text{Kerr})}} \frac{dx}{\Delta(x)}\right), \quad (48)$$

where $\Delta(x) = x^2 - 2Mx + a^2$ (for more details about the definition of r_{\min} see [21]). The odd correspondence between ξ and Boyer-Lindquist coordinate $r^{(\text{Kerr})}$ was chosen in order to transform the radial part of the wave equation into a form that is as close to that of Kerr as possible, and it is related to the fact that the radial coordinate in Kerr should not be interpreted as a spherical coordinate in flat space. For sufficiently large values of $r^{(\text{Kerr})}$ though, $r^{(\text{Euler})} \simeq r^{(\text{Kerr})}$, as it can be easily shown.

Therefore, not only the two problems lead to separable wave equations, but the corresponding eigenfunctions, on which any wave perturbation can be decomposed, are quite similar. More specifically the angular eigenfunctions are exactly the same, while the radial ones, although not identical, they have the same behavior at large radii.

5 Revealing new analogies

We devote this section in constructing an extended list of new analogies that demonstrate the close analogy between the relativistic gravitational field of Kerr space-time and the Newtonian gravitational field of the oblate Euler's problem.

5.1 Orbital precession

It is well known that a bound geodesic orbit around a Kerr metric, generally oscillates about the equatorial plane, while it revolves around the black hole. Thus an orbit with $L_z \neq 0$ never crosses the symmetry axis; but it oscillates within a maximum angular amplitude about the equatorial plane. This angle is called the inclination of the orbit (see [5]), and it could be easily obtained by computing the extreme angles, $\theta_{\min}, \pi - \theta_{\min}$, constraining the θ -oscillation. This is directly regulated by the value of Carter constant Q . Especially, for $Q = 0$ the orbit is strictly equatorial.

Since the connection between $\theta = \cos^{-1} \eta$, p_θ and Q for the Euler's problem (52) is exactly the same with that for Kerr (after adopting a redefinition of the constant $E \rightarrow (E^2 - 1)/2$, discussed in Section 3.2), the orbits of a test particle in the oblate Euler's problem will have similar azimuthal properties with those of Kerr. As long as an Euler orbit is characterized by $L_z \neq 0$, its θ (related to the spheroidal coordinate η) oscillates back and forth around zero, while the corresponding extreme values of θ are symmetrical to each other,

determining the inclination of the orbit. Again when the Carter constant Q of Euler vanishes, the orbit is equatorial.

Furthermore, in both problems, a bound orbit, while revolving around the axis of symmetry, and oscillating around the equatorial plane, it also moves radially in and out between two extremal radii ($r_{\min} \leq r \leq r_{\max}$). If these two radii are equal then we get a “circular” (or as we call it here “spherical”) orbit. In the Kerr case circular orbits have been shown to be stable against gravitational wave perturbations. Later on, we will demonstrate that this is not generally true for bound orbits in Euler. Although this is a qualitative difference between Kerr and Euler, this particular difference between the two problems enhances the qualitative similarity between the two problems, since the resonance condition on which the whole argument about stability is based, can be used for both problems. It happens that in the Euler case there are physical parameters for which the resonance condition holds true; consequently the corresponding spherical orbits become unstable. In Kerr case there is no such resonance for any bound orbit; thus spherical orbits are stable. Section 6 is especially devoted to demonstrate how this difference arises when applying the same argument in the two qualitatively similar problems.

Finally we should add that for both problems, usually there is a pair of bound orbits, one of which corresponds to actually plunging orbits in Kerr case (since such an orbit is partly buried beneath the horizon of the black hole). In contrast the Euler problem is not endowed with any horizons, thus this family of orbits are still regular orbits with lower extremal radii (r_4, r_3) than the corresponding extrema (r_1, r_2) corresponding to its normal counterpart orbit. To keep a close correspondence with Kerr orbits though, we will baptize this new family of orbits “plunging orbits” as well, and we will not study them furthermore.

As mentioned before, it should also be pointed out here that there is another fundamental difference between the two problems. In Kerr space-time the prograde orbits (orbiting at the same sense as the spin of the black hole) and retrograde orbits (orbiting at the opposite sense) are distinct; they have different characteristics. This is due to the Lense-Thirring effect caused by the spin of Kerr metric, and it arises due to the nonvanishing current-mass moments of the corresponding metric. The current-mass moments, though, are not present in a static Newtonian gravitational field; therefore the prograde and retrograde orbits are completely equivalent in the sense that they become identical under the transformation $\phi \rightarrow -\phi$. This qualitative

difference between the two fields is emphasized in those cases where the description of a phenomenon encompasses linear functions of a in the Kerr metric, while only the square of a shows up in the corresponding description of the Euler problem. When some particular property of the Kerr field, that differentiates a prograde from a retrograde orbit, is compared to the corresponding one of the Euler field, naturally, disagreements will appear. We will handle this comparison with great care by considering an average of a carefully chosen pair of orbits (consisting of one prograde and one retrograde), both characterized by the same physically measurable quantity (see below at Section 5.3).

5.2 The Carter-like constant

The Carter constant is a conserved quantity along the geodesics in Kerr space-time. In Boyer-Lindquist coordinates, when expressed in terms of p_θ momenta, it takes the following form:

$$Q = p_\theta^2 + \cos^2 \theta \left[a^2 (1 - E^2) + \frac{L_z^2}{\sin^2 \theta} \right] \quad (49)$$

while, when expressed in terms of p_r momenta, it takes a quite different form:

$$Q = \frac{[E(r^2 + a^2) - aL_z]^2}{\Delta} - (L_z - aE)^2 - r^2 - \Delta p_r^2, \quad (50)$$

where $\Delta = r^2 - 2Mr + a^2$. In the expressions above, E , L_z are the conserved energy ($-p_t$) and the conserved z -component of the angular momentum (p_ϕ) of an orbiting test particle. Both momenta are proportional to the particle's rest mass μ ; thus Q itself is proportional to μ^2 . Equivalently, one could construct the reduced quantities $\tilde{Q} = Q/\mu^2$, $\tilde{E} = E/\mu$, $\tilde{L}_z = L_z/\mu$, $\tilde{p}_\theta = p_\theta/\mu$, $\tilde{p}_r = p_r/\mu$, and rewrite the above expressions in terms of the corresponding reduced quantities, that are not related to the test particle, but only on the particular geodesic. For simplification we are going to use Eqs. (49, 50) themselves, without the tilde signs, but referring to the reduced quantities. This is equivalent to the quantities of a test particle with rest mass $\mu = 1$.

Earlier (in Section 3.2) we derived Euler's third integral of motion (c.f. Eqs. (41, 42)). By rewriting the energy E of the Euler field in terms of its relativistic analogue at the non-relativistic limit:

$$(E^{(K)})^2 = 2E^{(E)} + 1, \quad (51)$$

we get, after omitting the corresponding ^(K) marks, the following expressions for the Euler's Carter constant:

$$Q = p_\theta^2 + \cos^2 \theta \left[a^2(1 - E^2) + \frac{L_z^2}{\sin^2 \theta} \right], \quad (52)$$

in terms of θ, p_θ , and after some term rearrangement:

$$Q = \frac{[E(r^2 + a^2) - aL_z]^2}{r^2 + a^2} - (L_z - aE)^2 - r^2 - (r^2 + a^2)p_r^2 + 2Mr, \quad (53)$$

in terms of r, p_r . Although the second expression for Q could be written in a simpler form where the a parameter shows up solely through a^2 (the terms linear in a in Eq. (53) vanish if we expand it), we have chosen the above formulation in order to have a closer comparison with the corresponding expression for Kerr (see Eq. (50) above). Note that the first formula (52) has exactly the same form as the Carter constant of Kerr (49), while the second one (53), although quite similar (both are rational functions built from polynomials of the same order with respect to r), apparently it does not match exactly the form of Q for Kerr. However, it should be noted that the presence of the mass of the source, M , only at the last term of the expression (53) for Euler's Q , although it seems to have no analogue term in the corresponding expression for Q in Kerr, this is misleading. The presence of M in Δ in Eq. (50) will show up exactly as $2Mr$ when Δ in the denominator of the first term is expanded at lowest order with respect to M/r and assume that the particle moves at the weak gravitational field where $E \simeq 1$. Of course the two problems are not identical to each other, and this is the best analogy between the two expressions we could achieve. At the weak field limit though the similarity is even better.

5.3 The ISCO

The usual gravitational field of a Newtonian monopole lacks the analogue of an innermost stable circular orbit (ISCO) which is present in the gravitational field of a Schwarzschild black hole. The reason is that the centrifugal potential in Newtonian gravitational fields acts always as a repulsive potential which, compared to a suitably soft gravitational field like that of a Newtonian monopole, it ensures that there is always a stable circular orbit at any radius. This could be considered as a clear difference between the

relativistic (Kerr) and the Newtonian (Euler) gravitational field at the limit $a = 0$.

This fact is deceiving though. The Euler's problem has also an ISCO for any non-vanishing value of a . If one considers a circular orbit on the equatorial plane ($\theta = \pi/2$) of the Euler's oblate field, then the corresponding effective potential in cylindrical coordinates is

$$V_{\text{eff}} = \frac{L_z^2}{2\rho^2} + V(\rho, z = 0) = \frac{L_z^2}{2\rho^2} - \frac{M}{\sqrt{\rho^2 - a^2}}, \quad (54)$$

where L_z is the reduced z -angular momentum of the test particle (or the angular momentum for a unit mass particle). In terms of the oblate spheroidal coordinates instead, the above potential assumes the following form:

$$V_{\text{eff}}(\xi, \eta = 0) = \frac{L_z^2}{2a^2(\xi^2 + 1)} - \frac{M}{a\xi}. \quad (55)$$

By solving simultaneously the equations $V_{\text{eff},\xi} = V_{\text{eff},\xi\xi} = 0$, corresponding to the presence of an ISCO, leads to $\xi_{\text{ISCO}} = \sqrt{3}$. Thus the oblate Euler problem does have an ISCO, the actual radius of which in cylindrical coordinates is

$$\rho_{\text{ISCO}} = a\sqrt{\xi_{\text{ISCO}}^2 + 1} = 2a, \quad (56)$$

or in spheroidal radius

$$r_{\text{ISCO}} = a\xi_{\text{ISCO}} = \sqrt{3}a. \quad (57)$$

Note that r_{ISCO} is not the real Euclidean distance from the origin to the test particle at ISCO (the Euclidean distance is ρ_{ISCO}), but it is the analogue of the Boyer-Lindquist radius of Kerr, which we use extensively in our paper in order to draw a faithful comparison of Euler with Kerr.

Oddly enough, the existence of ISCO in the Euler problem is still present even in the limit $a \rightarrow 0$; the corresponding radius just tends to $r_{\text{ISCO}} = 0$ then. This is a new qualitative feature that the Newtonian monopole field ($a = 0$) lacks, as mentioned previously. Therefore, the case $a \rightarrow 0$ (but $a \neq 0$) could be considered as the analogue of a Schwarzschild black hole. Note, also, that contrary to oblate Euler problem, the original Euler problem (the prolate one) does *not* possess an ISCO. This is due to the fact that in the prolate Euler field the attraction from the two point sources, located

along the z -axis, is even softer than the Newtonian one from a single point source; therefore the repulsive centrifugal potential rules out the existence of an ISCO in this case.

The critical value of z -angular momentum leading to the presence of ISCO in the oblate Euler field is

$$L_z^2 = \frac{16Ma}{3\sqrt{3}}, \quad (58)$$

while the corresponding expression for the Kerr field is quite involved and difficult to compare with the above simple formula, since the expression of the z -angular momentum for a prograde and a retrograde orbit as a function of a is different, due to the Lense-Thirring effect.

Although the existence of an ISCO in the Newtonian problem is by itself a positive qualitative sign of the physical resemblance with the relativistic problem of a Kerr black hole, apparently it does not seem to share any quantitative similarity with the dependence of ISCO radius in Kerr with its spin parameter a (see [22]):

$$r_{\text{ISCO}} = M \left[3 + Z_2 \mp \sqrt{(3 - Z_1)(3 + Z_1 + 2Z_2)} \right], \quad (59)$$

where

$$Z_1 = 1 + (1 - a_\star^2)^{1/3} \left[(1 + a_\star)^{1/3} + (1 - a_\star)^{1/3} \right], \quad (60)$$

and

$$Z_2 = \sqrt{3a_\star^2 + Z_1^2}, \quad (61)$$

with $a_\star = a/M \in [0, 1]$ while the two signs correspond to prograde (upper sign) and retrograde (lower sign) orbits, respectively. As mentioned previously the a 's showing up in the expressions for the ISCO radius in the two problems have completely different physical origin: in Euler field it's just a distance, while in Kerr field it is related to the angular momentum of the gravitational source itself; therefore apart of the existence of an ISCO radius in both problems, no qualitative similar behavior of r_{ISCO} with a was anticipated. In Figure 3 the ISCO radii as a function of a_\star for both types of orbits in Kerr are plotted. The apparent non-linearity –especially for the prograde orbit–, in contrast to the linearity of the oblate Euler problem, is clear.

On the other hand the comparison between the two problems is not exactly fair from a physical point of view. The relativistic problem, although

axisymmetric, strongly discriminates between the two opposite senses of rotation of an orbit (it is not symmetric under the transformation $\phi \rightarrow -\phi$), while the Newtonian one is absolutely symmetric under such a transformation. Thus two circular equatorial orbits in Kerr that rotate at opposite senses at the same radius are not equivalent. It should be more appropriate to compare two orbits (a prograde and a retrograde one) with opposite rotational frequencies, after taking into account the frame-dragging of space-time itself, as in the case for two oppositely directed circular orbits in Euler's problem at the same radius. Of course such pairs of circular orbits in Kerr will not have the same radii; thus one should assign some kind of an average value of radius for such a pair of oppositely, equally rotating, orbits in Kerr. To compute the actual rotational frequencies in the Kerr metric, means that one should firstly subtract the rotational rate of space-time itself, that is the rotational rate of ZAMOs [23]. Then one should seek ISCO orbits with equal absolute values of rotational rates with respect to ZAMO observers, in order to nullify the relativistic effect of frame-dragging and put the oppositely directed orbits on equal footing. In order to accomplish such a comparison of ISCO radii between oblate Euler's problem and Kerr, we followed the following process: (i) For the Kerr case, first we plotted $\Omega_{\text{phys}} = |\omega - \Omega_{\text{ZAMO}}|$ at the radius of ISCO as a function of a_* for both prograde and retrograde orbits (see Figure 4). It is clear that the retrograde orbits have monotonically decreasing rotation rate with a_* , which qualitatively follows a similar behavior with the rotation rate of circular Keplerian orbits $\Omega \propto r^{-3/2}$, while r_{ISCO} is increasing with a_* . Instead, the rotation rate of prograde orbits have completely different dependence on a_* . These orbits lie so deep in the strong gravitational field of the black hole and the frame-dragging effect is then so dramatic (the region close to $a_* = 1$ is actually buried inside the ergoregion which has no analogue in Newtonian gravity), that their behavior with respect to rotational frequency is completely different from those in the Newtonian problem. More specifically, there is no corresponding retrograde ISCO orbit that rotates at the same rate (relative to ZAMO observers) for almost any prograde ISCO orbit, except of the prograde ISCO orbits at large, but not extremal ($a_* \simeq 1$), values. The range of a'_* 's of prograde orbits with a corresponding dual retrograde orbit, sharing the same Ω_{phys} , is $0.760 \leq a'_* \leq 0.838$. On the other hand for any retrograde ISCO orbit (corresponding to any value of $a_* \in [0, 1]$) there is a corresponding prograde one (one with the same value of $|\omega - \Omega_{\text{ZAMO}}|$). Therefore we could form pairs of retrograde-prograde orbits with the same physical rotation rate $\Omega_{\text{phys}} = |\omega - \Omega_{\text{ZAMO}}|$. On each such

pair we assigned the a_\star of the retrograde one (since this is the one that has a counter-rotating dual with some a'_\star value, for every value of a_\star). (ii) Then we numerically computed the r_{ISCO} 's for both orbits (the retrograde (R) corresponding to a_\star and the prograde (P) corresponding to a'_\star , both characterized by the same Ω_{phys}). (iii) For each such pair we computed the average value of ISCO radii, $\langle r_{\text{ISCO}} \rangle$, according to the relation

$$\langle r_{\text{ISCO}} \rangle(a_\star) = \frac{1}{2} \left(r_{\text{ISCO}}^{(R)}(a_\star) + r_{\text{ISCO}}^{(P)}(a'_\star) \right) \quad (62)$$

that takes into account the two radii of the oppositely rotating orbits on equal footing. (iv) Finally we have plotted $\langle r_{\text{ISCO}} \rangle$ as a function of a_\star and the output was apparently almost linear (see Figure 5), like in the Euler case.

Although it might seem rather artificial the way the $\langle r_{\text{ISCO}} \rangle$ was defined, we believe there is actually no other way to define a radius of ISCO that treats both the retrograde and the prograde orbits on equal footing as it is always the case with axisymmetric Newtonian problems. The only alternative natural way we could think of in order to form pairs of equivalent oppositely directed orbits is by assuming orbits with equal absolute values of angular momenta, instead of orbital frequency. We tried that as well but there is no pair of retrograde-prograde orbits with the same value of $|L_z|$. In contrast to Ω_{phys} , $|L_z(a_\star)|$ is a monotonic function of a_\star , for $a_\star \in [-1, 1]$, where the sign of a_\star determines the rotational direction of the orbit. The deeper reason is that the frame-dragging effect is so enhanced for large values of a_\star that one needs extreme value of angular momentum to keep a circular orbit stable, when it lies deep in the gravitational potential.

For completeness, we should note that the above method to construct equivalent pairs of prograde and retrograde orbits, leads to a double solution only for the case of $a_\star = 0$, since then there are two a'_\star values for a prograde orbit with the same $|\omega - \Omega_{\text{ZAMO}}|$ of a corresponding retrograde orbit; one of them being the zero spin case. For continuity reasons though, we have ignored the second root –that of zero spin.

As we mentioned earlier, the dependence of ISCO radius of the Euler's problem on a_\star parameter, is linear (c.f. Eq. 57)). Amazingly, this is approximately the behavior of $\langle r_{\text{ISCO}} \rangle$ in Kerr case with respect to the spin parameter a_\star , when a retrograde and a prograde orbit are considered as a suitably equivalent pair. A last comment on this similarity is that quantitatively the approximate linear fashion of $\langle r_{\text{ISCO}} \rangle$ with a_\star in Kerr, although of

the same order, it does not have the same slope with that of Euler, which is $\sqrt{3}$.

To further stress this peculiar equivalence of oppositely rotating orbits in Kerr, we have also plotted the square of the average value of L_z 's for each such pair of equally rotating orbits as a function of a_* (see Figure 6). Apparently this plot is also almost linear as in the Euler case, according to Eq. (58). The corresponding slopes though are remarkably different.

5.4 The fundamental frequencies

The Euler potential is an integrable system with three independent and in involution integrals of motion. The conjugate momenta p_r and p_θ (cf. Eqs. (42) and (41)) are functions only of r , and θ , respectively. For bound orbits (see Section 3.2), the space of trajectories is a compact and connected manifold. According to Arnold's theorem [10], the phase space is diffeomorphic to a three-torus. Since the problem is integrable, even though the coordinates are not really periodic, their oscillation (or libration for ϕ) correspond to characteristic frequencies, the so called fundamental frequencies.

Consequently, we could define a set of symplectic coordinates, the corresponding action-angle variables $(\mathbf{J}, \boldsymbol{\omega})$, where the angle variables $\boldsymbol{\omega}$ are periodic functions of time, and the action variable \mathbf{J} corresponds to a fixed vector. The three frequencies related to the periodicities of $\boldsymbol{\omega}$'s are the fundamental frequencies that one obtains by Fourier analyzing the oscillating (or librating) time dependence of the coordinates r, θ and ϕ coordinates of a bound orbit.

The generating function of the canonical transformation $(q_i, p_i) \rightarrow (J_i, \omega_i)$ is the Hamilton's characteristic function $W(\mathbf{q}, \mathbf{F})$, which is the solution of Hamilton-Jacobi equation $\partial S / \partial t + H(q_i, \partial S / \partial q_i) = 0$:

$$S(q_i, F_i, t) = -Et + W(q_i, F_i), \quad (63)$$

where q_i are the old coordinates (r, θ, ϕ) and their conjugate momenta p_i are defined as: $p_r = \pm \sqrt{V_r(r) / (r^2 + a^2)}$, $p_\theta = \pm \sqrt{V_\theta(\theta)}$, and $p_\phi = L_z$, (the corresponding potentials V_r, V_θ are given explicitly in Eqs. (37, 38)). The first integrals of motion are: $F_i = (H = E, L_z, Q)$. Due to the separability of the Hamilton-Jacobi equation its solution is of the form:

$$W(\mathbf{q}, \mathbf{F}) = L_z \phi \pm W_r(r) \pm W_\theta(\theta), \quad (64)$$

where:

$$W_r(r) = \int^r \frac{\sqrt{V_r}}{r^2 + a^2} dr, \quad (65)$$

$$W_\theta(\theta) = \int^\theta \sqrt{V_\theta} d\theta. \quad (66)$$

The action variables are defined as (see [10]):

$$J_i = \frac{1}{2\pi} \oint p_i dq_i, \quad (67)$$

where the integration is to be carried over a period of oscillation or rotation of q_i .

The action variables J_i are constants of motion, as they depend only on the first integrals $J_j = J_j(F_i)$. Inverting them we can express the integrals F_i as functions of the action variables. In particular the Hamiltonian can be expressed as $H = F_1 = H(\mathbf{J})$ and it is cyclic with respect to ω_i . The generating function also can be expressed in terms of the coordinates and the action variables:

$$W = W(\mathbf{q}, \mathbf{J}). \quad (68)$$

The transformation equations are:

$$p_i = \frac{\partial W}{\partial q_i}(\mathbf{q}, \mathbf{J}), \quad (69)$$

$$\omega_i = \frac{\partial W}{\partial J_i}(\mathbf{q}, \mathbf{J}), \quad (70)$$

while the equations of motion in action-angle variables become:

$$\dot{\omega}_i = \frac{\partial H(\mathbf{J})}{\partial J_i} = \Omega_i, \quad (71)$$

$$\dot{J}_i = -\frac{\partial H(\mathbf{J})}{\partial \omega_i} = 0. \quad (72)$$

The corresponding angle variables are periodic and linear functions of time:

$$\omega_i(t) = (\Omega_i(\mathbf{J})t + \omega_i(0)) \mod 2\pi \quad (73)$$

where $\Omega_i(\mathbf{J})$ and $\omega_i(0)$ are constants and $\Omega_i(\mathbf{J}) = \partial H(\mathbf{J})/\partial J_i$ describe the fundamental frequencies of the orbit. In Appendix D we give analytic expressions of the above quantities, J_i, Ω_i . Here we simply give the final expressions:

$$\Omega_r = \frac{\pi K(k)}{a^2 z_+ [K(k) - E(k)]X + YK(k)} \quad (74)$$

$$\Omega_\theta = \frac{\pi \beta \sqrt{z_+} X/2}{a^2 z_+ [K(k) - E(k)]X + YK(k)} \quad (75)$$

$$\Omega_\phi = \frac{ZK(k) + XL_z[\Pi(\frac{\pi}{2}, z_-, k) - K(k)]}{a^2 z_+ [K(k) - E(k)]X + YK(k)} \quad (76)$$

where $K(k)$, $E(k)$ and $\Pi(z_-, k)$ are the complete elliptic integrals of the first, second and third kind, respectively [24]:

$$K(k) = \int_0^{\frac{\pi}{2}} \frac{d\theta}{\sqrt{1 - k^2 \sin^2 \theta}}, \quad (77)$$

$$E(k) = \int_0^{\frac{\pi}{2}} \sqrt{1 - k^2 \sin^2 \theta} d\theta, \quad (78)$$

$$\Pi(z_-, k) = \int_0^{\frac{\pi}{2}} \frac{d\theta}{(1 - z_- \sin^2 \theta) \sqrt{1 - k^2 \sin^2 \theta}}, \quad (79)$$

with $k = \sqrt{z_-/z_+}$ (where z_\pm are the two roots of $V_\theta(\cos \theta)$, with $z_- < 1 < z_+$) and $\beta^2 = -2a^2 E$. The integrals X , Y and Z are related with the radial motion and are defined as:

$$X = \int_{r_1}^{r_2} \frac{dr}{\sqrt{V_r}}, \quad (80)$$

$$Y = \int_{r_1}^{r_2} \frac{r^2}{\sqrt{V_r}} dr, \quad (81)$$

$$Z = \int_{r_1}^{r_2} \frac{L_z r^2}{(r^2 + a^2) \sqrt{V_r}} dr, \quad (82)$$

with V_r being the radial potential $V_r(r)$ introduced in Eq. (37).

Although the orbit is not periodic, there are specific cases, where the motion is clearly periodic. A resonant orbit, where the ratio $\Omega_r \div \Omega_\theta \div \Omega_\phi$ is a ratio of integers, is a more involved case of a purely periodic orbit since then an integer number of oscillations of θ , r and ϕ (not necessarily the same numbers) are repeated in a finite time period.

For comparison the fundamental frequencies of a bound orbit in Kerr space-time have been derived by Schmidt [25] and they are given by exactly the same expressions with that of Euler (74)-(76), with $\beta^2 = a^2(1 - E^2)$ and z_{\pm} the two roots of the Kerr polar potential (which is the same with the polar potential of Euler). The radial integrals for Kerr though are given by (see [25]):

$$\begin{aligned} X &= \int_{r_1}^{r_2} \frac{dr}{\sqrt{V_r}}, \\ Y &= \int_{r_1}^{r_2} \frac{r^2}{\sqrt{V_r}} dr, \\ Z &= \int_{r_1}^{r_2} \frac{L_z r^2 - 2Mr(L_z - aE)}{(r^2 - 2Mr + a^2)\sqrt{V_r}} dr, \end{aligned}$$

where the corresponding potential V_r is

$$\begin{aligned} V_r = & (E^2 - 1)r^4 + 2Mr^3 + [(E^2 - 1)a^2 - Q - L_z^2] r^2 \\ & + 2M [(L_z - aE)^2 + Q] r - Qa^2. \end{aligned}$$

If we rewrite the Newtonian energy of the V_r potential of Eq. (37) as previously: that is by adopting the reparametrization $2E \rightarrow E^2 - 1$, we obtain a form of the radial potential of Euler which differs from that of Kerr only on the linear term. Therefore whatever differences in frequencies between the Kerr and the Euler field, arise from this difference in V_r and the different expression of the Z integral.

In Kerr space-time there is also a fourth constant Ω_t which is associated with the generalized time coordinate. However, the motion is not bounded in the timelike direction, so Ω_t cannot be interpreted as a physical fundamental frequency [25, 26].

5.5 Pairs of isofrequencies

Warburton et al [27] have shown that Kerr black holes (Schwarzschild black holes included) have an interesting property: there is no one-to-one correspondence between orbital characteristics and fundamental frequencies, that is, there are pairs of distinct bound geodesic orbits lying in the strong field region, that are characterized by exactly the same triplets of frequencies (radial, azimuthal, and longitudinal). Motivated by the fact that the oblate

Euler field has an ISCO, like the gravitational field of a Kerr black hole, we looked for pairs of distinct, potentially synchronized, orbits in the Euler field as well.

Following the procedure of [27], we first searched for pairs of equatorial orbits with equal doublets of (Ω_r, Ω_ϕ) frequencies. While the third frequency, Ω_θ , could also be computed for such orbits, it does not show up in the orbital motion, since the orbit is purely equatorial. In order to seek such double solutions in the frequency space, we have plotted the contours of $\Omega_r = \text{const}$ in the (e, Ω_ϕ) plane. Actually the very shape of the boundary of all possible equatorial orbits in the parameter space mentioned above, namely the contour-curve corresponding to $\Omega_r = 0$, is sufficient to ensure the existence of pairs of orbits with the same set of (Ω_r, Ω_ϕ) frequencies. The boundary consists of orbits: (i) with infinite semi-latus rectum p , corresponding to $\Omega_\phi = 0$, but with various eccentricities (infinitely distant bound orbits), (ii) with eccentricity $e = 1$ (marginally closed orbits), corresponding to a range of Ω_ϕ frequencies depending on the semi-latus rectum, and (iii) the separatrix, that is, orbits corresponding to a potential $V_r(r)$ with a double root $r_2 = r_3$ (and $V'_r(r_2) = 0$), such that the orbit spends infinite time to complete an r -oscillation between r_1 and r_2 . The ISCO is simply the endpoint of the separatrix at $e = 0$, corresponding to a marginally stable circular orbit, due to a suitable tuning of the polynomial expression for the potential V_r , to obtain a triple root, $r_1 = r_2 = r_3 = \sqrt{3}a$ (see Section 5.3). Along the separatrix of equatorial orbits, Ω_ϕ is given by the simple expression

$$\Omega_{\phi,s}^{(\text{eq})} = \sqrt{\frac{M}{r_2^3}}, \quad (83)$$

where $r_2 = p/(1 + e)$, since the particle will eventually end up to radius r_2 . Following Eq. (144) of Appendix C, the ϕ -frequency of such orbits could be expressed as:

$$\Omega_{\phi,s}^{(\text{eq})} = \left(\frac{1+e}{3-e}\right)^{3/4} \sqrt{\frac{M}{a^3}}. \quad (84)$$

The separatrix has positive slope, $de/d\Omega_\phi|_s > 0$. Consequently, the boundary of the contour plot, $\Omega_r = 0$, forms an inverted trapezoid (as in Kerr) in the parameter space $(e - \Omega_\phi)$. Due to continuity of the function $\Omega_r(e, \Omega_\phi)$ for equatorial orbits, this shape is conclusive for the existence of isofrequency pairs of orbits (see Figure 7), as pointed out also in the case of Kerr [27].

In Appendix C we give analytic formulae for the constants of motion at the separatrix and from them one could compute, based on the expressions of Appendix D, the fundamental frequencies for these peculiar marginally whirling equatorial orbits. Apart of the separatrix, the bound equatorial orbits exhibit the following characteristics: (i) There is a maximum value of Ω_r , which corresponds to a circular orbit ($e = 0$), marked as ‘c’ in the contour plot of Ω_r , Figure 7. The analytic expression for Ω_r at zero eccentricity is simply

$$\Omega_r(p, e = 0) = \frac{\sqrt{p^2 - 3a^2}}{p^{5/2}} \sqrt{M}. \quad (85)$$

Thus the maximum value of $\Omega_r(p, e)$ is $\Omega_{r,c} = \sqrt{2/5^{5/2}} \sqrt{M/a^3}$, for $p_c = \sqrt{5}a$ and $e = 0$. (ii) There is a line of non-circular orbits, called ‘COD’ curve (circular orbit duals) in [27], that have the same frequency set, (Ω_r, Ω_ϕ) , with a single corresponding circular orbit. The range of Ω_ϕ ’s that the COD curve spans is $[\Omega_{\phi,b}, \Omega_{\phi,i}]$, corresponding to specific circular orbits marked as ‘b’, ‘i’ in the parameter space, respectively. The ‘i’ circular orbit is simply the ISCO orbit, representing the maximum Ω_ϕ value of a circular orbit (with $e = 0$), the dual of which is a non-circular orbit with $e = 1$ (the upper end-point of the green dashed curve of Figure 7). On the other hand ‘b’ is the circular equatorial orbit with a non-circular dual which has the lowest Ω_ϕ and the highest Ω_r that such an orbit could yield. The ‘b’ circular orbit is actually a singular case since the twin pair of the corresponding circular orbit is exactly the same orbit, representing now a marginally non-circular orbit. On the left side of the COD curve one could find all possible iso-frequency pairs. (iii) Finally, there is another special curve representing all iso-frequency pairs with marginally equal orbital parameters. Along this curve the Jacobian of the transformation between the frequency parameter space and the orbital parameter space $(\Omega_r, \Omega_\phi) \rightarrow (p, e)$ vanishes, which means that the transformation is singular: each point along this line corresponds to a double root of the system of equations

$$\begin{aligned} \Omega_r(p, e) &= \Omega_{r0}, \\ \Omega_\phi(p, e) &= \Omega_{\phi0}. \end{aligned} \quad (86)$$

This curve joins the points of the iso- Ω_r contour lines that represent the extremum values of Ω_ϕ for each Ω_r . This singular curve spans all eccentricities from marginal bound orbits ($e = 1$) to circular orbits ($e = 0$) meeting the COD line at point ‘b’. As mentioned above, point ‘b’ represents a singular

circular orbit which is the dual of itself. The other end-point of the singular curve (the left-most corner of the plot in Figure 7) corresponds to the highest possible Ω_ϕ value for any bound orbit, and it is denoted as ‘ w ’ in the contour plot. Since this orbit is an orbit at the separatrix, its semi-latus rectum is $p_w = 2a$ (this is what one yields from the parametric Eq. (144) when the values $e = 1$ and $x = 0$ are imposed), while its corresponding Ω_ϕ frequency is $\Omega_{\phi,w} = \sqrt{M/r_2^3} = \sqrt{M/a^3}$.

In order to plot the singular curve we have to solve the equation

$$J = \left| \frac{\partial(\Omega_r, \Omega_\phi)}{\partial(p, e)} \right| = 0. \quad (87)$$

The Jacobian of the transformation was computed numerically for arbitrary eccentricities. However the base of this line, ‘ b ’, corresponding to zero eccentricity was derived analytically since then the complicated functions $\Omega_\phi(p, e)$, and $\Omega_r(p, e)$, could be written as simple analytical expressions, when expanded as Taylor series around $e = 0$. Both frequencies yield the form $\Omega_0(p) + e^2\Omega_2(p)$. Therefore the Jacobian of the transformation is linear with respect to e near $e = 0$. This explains why all iso- Ω_r contours are intersecting the Ω_ϕ -axis at right angles; that is, a slight eccentricity $e \ll 1$ does not alter both frequencies of the corresponding circular orbits at order $O(e)$. More specifically, the Jacobian determinant of the transformation near $e = 0$ yields the following form

$$J|_{e \rightarrow 0} = \left| -\frac{9Ma^2(5a^4 - 15a^2p^2 + 4p^4)e}{4p^5(p^2 - 3a^2)^{3/2}(p^2 + a^2)} + O(e^2) \right|. \quad (88)$$

Thus the starting point ‘ b ’ of the COD line (at $e = 0$), which coincides with the starting point of the singular line, is given by the solution of the algebraic equation $5a^4 - 15a^2p^2 + 4p^4 = 0$, which is

$$p_b = a\sqrt{(15 + \sqrt{145})/8} \simeq 1.839a,$$

(the second solution is lower than the ISCO radius so it has been omitted; this corresponds to the semi-latus rectum of the dual plunging orbit that lies beyond the separatrix). Finally, from the semi-latus rectum one can compute the two frequencies $\Omega_{\phi,b}$, and $\Omega_{r,b}$. The numerical values of these frequencies are $\Omega_{r,b} \simeq 0.135\sqrt{M/a^3}$ and $\Omega_{\phi,b} = 0.401\sqrt{M/a^3}$.

In Table 1 we summarize the above results by presenting a complete list of the values of all characteristic frequencies discussed in the previous paragraph

(all are simply multiples of the dimensional quantity $\sqrt{M/a^3}$), as well as the corresponding semi-lata recta, p , of these orbits. It should be emphasized that not only the characteristic frequencies, but the frequencies of any bound orbit in the Euler field, are all scaled with $\sqrt{M/a^3}$, independently of a and M ; they depend only on the characteristic orbital parameters e and $p_\star = p/a$. Therefore the contour plot of Figure 7 does not represent a specific a value, as in the Kerr case. In contrast the exact form of the contour curves in Kerr does depend on a , due mainly to the dragging of frames in the corresponding relativistic problem. The shape of the Ω_r -contour lines on the left of the COD line ensures that one could find pairs of equatorial orbits with different orbital parameters but with the same set of frequencies. Two such orbits have been plotted in Figure 8 and have been marked (as A and B) on the

	c	b	i	w
Ω_r^\star	0.189	0.135	0	0
Ω_ϕ^\star	0.299	0.401	0.439	1
p^\star	2.236	1.839	1.732	2
e	0	0	0	1

Table 1: The characteristic frequencies in the $(e-\Omega_\phi)$ parameter-space for the equatorial Eulerian orbits. The Ω^\star 's are simply the dimensionless frequencies that arise when frequencies are written in terms of $\sqrt{M/a^3}$. These numerical values are independent of a . p^\star 's are the dimensionless semi-lata recta (p/a).

	A	B
Ω_r^\star	0.0790569	
Ω_ϕ^\star	0.453379	
e	0.5370696	0.2
p^\star	1.94569	1.83337

Table 2: The two orbits, marked as A and B in Figure 7, have been isolated in the region where iso-frequency pairs exist. One of them (B) was fixed and the other one was tracked down by numerically solving the complicated equation $\Omega_r(e, \Omega_\phi(p, e)) = \Omega_\phi(p, e) = \Omega_r(e_B, \Omega_\phi(p, e_B))$ with respect to e and p . All frequencies are scaled with the dimensional quantity $\sqrt{M/a^3}$, that is $\Omega_i = \Omega_i^\star \sqrt{M/a^3}$, while the semi-latus rectum p^\star is p/a .

contour plot of Figure 7.

There is also one more similarity connected with the orbital frequencies. The Schwarzschild gravitational field is a specific case of a Kerr metric, the orbits of which are not closed due to different values of Ω_ϕ and Ω_r . Also the Euler field, even when $a \rightarrow 0$, has orbits that are not closed, as well, (the ratio Ω_r/Ω_ϕ is not identically equal to unity and depends only on e and p/a and not on the actual value of a). Therefore this $a \rightarrow 0$ Euler field has orbital characteristics that are closer to Schwarzschild than to Kepler. The existence of ISCO in the, almost Newtonian, Euler field is a singular outcome of the above diversity of frequencies.

Next we investigate the existence of iso-frequency pairs in generic, non-equatorial orbits in the Euler gravitational field. Such orbits are characterized by a triplet of frequencies, $\Omega_r, \Omega_\theta, \Omega_\phi$, all of which are present in the evolution of the orbit. In this case it is quite more complicated to seek for a pair of orbits having the same triplet of frequencies $(\Omega_r, \Omega_\theta, \Omega_\phi)$, since the 3-dimensional parameter space $(e - \Omega_\theta - \Omega_\phi)$, spanned by all types of bounded orbits has the shape of a skewed triangular prism, which is so thin that it looks like a 2-dimensional slice in the parameter space (see Figure 9). The separatrix of these orbits is now a strip parametrized by the functions $\Omega_\theta(\zeta, e)$, $\Omega_\phi(\zeta, e)$, where ζ is a single parameter that varies the inclination of the orbit, while it adjusts the semi-latus rectum p , so that $r_2 = r_3$, at any given value of the eccentricity. This strip spans the whole range of eccentricities from $e = 0$ to $e = 1$. Even though the two frequencies $\Omega_\theta, \Omega_\phi$ increase monotonically as one moves from $e = 0$ to $e = 1$, for any given inclination of the orbit (the strip has the right slope to allow for iso-frequency pairs), this is not sufficient to ensure that there are iso-frequency pairs. The contour surfaces of constant Ω_r are also strips that fill, like onion-shells, the whole prism-like 3-D body of orbits in the new parameter space. If we intersect these iso- Ω_r contour surfaces, with the plane of constant Ω_ϕ (or one of constant Ω_θ), the intersection will not necessarily span the whole range of eccentricities $0 \leq e \leq 1$, due to the obliqueness of the body of orbits and its tiny thickness. This renders the search for iso-frequency pairs unattainable for a wide range of frequencies. More specifically, if one starts from an orbit in the region close to the separatrix and moves upwards (towards higher e) or downwards (towards lower e) in order to find its potential iso-frequency pair, one may end up at the oblique lateral boundary of the space of orbits, before reaching the initial Ω_r value. This potential failure is strengthened by the fact that the thickness of the 3-dimensional body, describing all possible

orbits in the parameter space, is extremely tiny. Therefore the starting point of this exploration might be quite essential. The search should only be restricted in a region close to that part of the separatrix strip that lies near the surface which plays the role of the singular line of equatorial orbits. Then a numerical computation of the frequencies in the neighborhood of that initial point follows. Our investigation ended up in the contour plot of Figure 10, which depicts a segment of the iso- Ω_r contours on the intersection of the parameter space with the plane $\Omega_\phi = 0.632456\sqrt{M/a^3}$. Due to the very narrow width of the parameter space, the horizontal axis covers a very small range of Ω_θ frequencies. This contour plot diagram looks like Figure 6 of [27] referring to generic orbits in Kerr. However, there is a small difference: in the Euler field the iso- Ω_r contours lie at higher Ω_θ values than those at the separatrix, while in Kerr the relative position is the opposite. The reason is that the separatrix surface is differently oriented with respect to the rest orbits in the three-dimensional parameter space $\Omega_\theta, \Omega_\phi, e$ in Kerr and in Euler; thus the rest of the bound orbits lie on opposite sides of the separatrix surface in the two problems.

Following, then, the numerical scheme we used in the equatorial orbits, we pinpointed two distinct orbits with the same triplet of frequencies (the two points along the same iso- Ω_r contour line of Figure 9). The orbital characteristics of these two orbits have been written in Table 3, while the r -, θ -, and $(\phi - \Omega_\phi t)$ -oscillations of these orbits, along with the orbits themselves, have been depicted in Figure 11.

	A	B
Ω_r^*	0.0455368	
Ω_ϕ^*	0.632456	
Ω_θ^*	1.08005	
e	0.25	0.116833918947677
p^*	1.48957	1.33702
$\theta_{\min}(^{\circ})$	70.148692322964	67.94240594

Table 3: These are the characteristics (orbital parameters and fundamental frequencies) of the pair of orbits shown up in Figures 10 and 11. Frequencies are given in units of $\sqrt{M/a^3}$ and the semi-latus recta in a units. The two orbits have different orbital characteristics, but their fundamental frequencies are exactly (up to a numerical accuracy of 80 significant figures) the same.

Note that for non-equatorial orbits, as well as for equatorial orbits, all frequencies could be written in terms of the dimensional quantity $\sqrt{M/a^3}$, that is the numerical value of all frequencies that multiplies $\sqrt{M/a^3}$, is independent of the actual value of a and M . This is the reason why we have not assigned any specific value of a in any of the plots of Figures 9, 10.

6 “Circular” orbits remain circular

In this section we will exploit the great similarity of the Euler’s potential with the Kerr field in order to investigate the stability of spherical orbits (the “circular orbits” of Kerr as they are mostly known) in both problems. The initial argument in favor of this proposition, for the Kerr case, was given by Ori and Kennefick [12] back in the 90’s. The argument was analytical, but rather obscure, while the resonance case $\Omega_r = 2\Omega_\theta$, which was the condition for the argument not to hold, was not further studied. Later on, in the late 90’s Ryan [28] presented an elegant argument for the stability, when the resonant condition is not met, based simply on the basic symmetries of Kerr.

Here we will present an extensive analytic argument to explain this stability, constructed in terms of the Euler problem. The argument could be recast, though, in the form of the Kerr case. In our study we have managed to translate the problem in a driven harmonic oscillator which has a continuously increasing amplitude when the above resonance condition is met. Especially the Euler case, in contrast to Kerr case, could be set at such an initially spherical condition that the resonance condition is met. We have shown that such an orbit will eventually deviate from sphericity when a generic dissipative self-force is taken into account. This is an example that strongly supports and further explores the “spherical stability” proposition.

Let us write down the equation of motion for the r coordinate of a particle in an Euler field in terms of Mino time λ (c.f. Eq. (166) of Appendix E), amended by a tiny extra force that drives adiabatically the particle away from its geodesic orbit:

$$\begin{aligned}\frac{d^2 r}{d\lambda^2} &= \frac{d}{d\lambda} \left(\pm \sqrt{V_r(r)} \right) + \epsilon F_r^{(SF)} \\ &= \frac{1}{2} V_r'(r) + \epsilon F_r^{(SF)}\end{aligned}\tag{89}$$

where $'$ denotes a derivative with respect to r , ϵ is a small parameter, analogous to μ^2/M of an EMRI (μ is the test-particle’s mass, while M is the

total mass of the Eulerian gravitational field). This is the usual scale of the relativistic gravitational self-force at lowest order. This force plays the role of the self-force of a relativistic test-particle orbiting around a Kerr black hole.

The potential V_r , related to orbital r -oscillation, is the quartic polynomial of r of Eq. (37), with coefficients that are given as functions of the three integrals of motion E, L_z, Q (of the geodesic equation), which are not constant anymore. Thus

$$V_r(r) = a_4 r^4 + a_3 r^3 + a_2 r^2 + a_1 r + a_0 \quad (90)$$

with $a_i = a_i(E, L_z, Q)$; thus

$$\frac{d^2 r}{d\lambda^2} = \left(2a_4 r^3 + \frac{3}{2}a_3 r^2 + a_2 r + \frac{1}{2}a_1 \right) + \epsilon F_r^{(SF)}. \quad (91)$$

Furthermore, the potential is characterized by a local minimum r_0 , around which the orbit evolves, at least initially. Thus $r(\lambda) \simeq r_0$, and $V'_r(r_0) = 0$. r_0 is the instantaneous center of r -oscillations, the amplitude of which is directly related to the eccentricity of the orbit (which is assumed extremely small at the beginning). Subtracting from the equation above the vanishing derivative of the potential at r_0 we obtain the following equation:

$$\begin{aligned} \frac{d^2 r}{d\lambda^2} &= 2a_4(r^3 - r_0^3) + \frac{3}{2}a_3(r^2 - r_0^2) + a_2(r - r_0) + \epsilon F_r^{(SF)} \\ &= (r - r_0) \left(2a_4(r^2 + rr_0 + r_0^2) + \frac{3}{2}a_3(r + r_0) + a_2 \right) + \epsilon F_r^{(SF)}. \end{aligned} \quad (92)$$

At this point it should be emphasized that the new parameter r_0 showing up in the last expressions could also be considered a function of E, L_z , and Q , since it is simply the maximum root of the cubic equation $V'_r(r) = 0$, which could be directly expressed in terms of a_1, a_2, a_3, a_4 .

If the corresponding geodesic orbit ($\epsilon = 0$) is initially almost “spherical”, that is $r(\lambda) \simeq r_0$, the equation above describes an approximate harmonic oscillator with $\omega_r^2 = -6a_4 r_0^2 - 3a_3 r_0 - a_2$, which oscillates with very small amplitude. (Note that this ω_r is simply the Y_r part of the fundamental frequency Ω_r mentioned in Appendix E, since it is the frequency with respect to Mino-time λ). However, when self-force is present, a_i ’s (consequently r_0 ,

as well), will evolve as mentioned previously; therefore $r(\lambda)$ will adiabatically deviate somehow from its pure oscillatory fashion.

In order to study the new type of evolution when any type of self-force is present, we will seek a solution in the form of

$$r(\lambda) = r_0(0) + e_0 \Delta(\lambda), \quad (93)$$

assuming $r_0(0)$ is the initial value of r_0 (the instantaneous minimum of V_r) and e_0 is the initial amplitude of r -oscillations (which is proportional to the small initial eccentricity of the orbit), while $\Delta(\lambda)$ is a function of λ , of order zero (while eccentricity e and magnitude of self-force ϵ are assumed to be of order one) that describes the overall evolution of r (both oscillatory and secular evolution). By direct replacement in Eq. (92) we obtain the following equation of motion with respect to Δ :

$$e_0 \frac{d^2 \Delta}{d\lambda^2} = -(r(\lambda) - r_0(\lambda)) \omega_r^2(\lambda) + \epsilon F_r^{(SF)}, \quad (94)$$

where $\omega_r^2(\lambda)$ is the instantaneous value of $-6a_4 r_0^2 - 3a_3 r_0 - a_2$, due to adiabatic changes of all these parameters.

Assuming ϵ, e are two comparable small quantities, as mentioned above, we will only keep quantities of order $O(e)$ and $O(\epsilon)$ in the equation above, and after using the full expression for $r(\lambda)$ from Eq. (94) we get:

$$\frac{d^2 \Delta}{d\lambda^2} = -\omega_r^2 \Delta - \frac{(r_0(0) - r_0)}{e_0} \omega_r^2 + \frac{\epsilon}{e_0} F_r^{(SF)}, \quad (95)$$

where we remind that the quantities Δ, ω_r, r_0 are functions of λ .

Next we will further analyze the drift of r_0 , $\delta r_0 \equiv r_0 - r_0(0)$, caused by the self-force. Since, by the definition of r_0 , $V_r'(r_0) = 0$ (where V_r is a function of r and λ —through the λ -dependence of its coefficients):

$$\begin{aligned} 0 &= V_r'(r_0(\lambda), \lambda) \\ &= V_r'(r_0(0) + \delta r_0, \lambda) \\ &\simeq V_r'(r_0(0), \lambda) + V_r''(r_0(0), \lambda = 0) \delta r_0, \end{aligned} \quad (96)$$

the drift of r_0 , δr_0 , is approximately given by

$$\delta r_0 \simeq -\frac{V_r'(r_0(0), \lambda)}{V_r''(r_0(0), \lambda = 0)} = \frac{0 + \delta V_r'(r_0(0), \lambda)}{2\omega_r(0)^2}, \quad (97)$$

where δV_r denotes the shift of V_r due to the evolution of the coefficients of its polynomial expression, while the initial value 0 at the numerator marks simply the value of the derivative of the initial (at $\lambda = 0$) V_r , at $r_0(0)$. The denominator $V_r''(r_0(0), \lambda = 0)$ has been directly replaced by its value, $-2\omega_r(0)^2$ (see the paragraph after Eq. (92)), calculated at the initial form of V_r .

By replacing δr_0 in Eq. (95) with our final answer, and neglecting the drift of ω_r^2 with λ in the second term of the right hand side, as a higher order term, we obtain

$$\frac{d^2\Delta}{d\lambda^2} = -\omega_r^2\Delta + \frac{\delta V_r'(r_0(0), \lambda)}{2e_0} + \frac{\epsilon}{e_0}F_r^{(SF)}. \quad (98)$$

Next, we will show that the value of the evolved V_r' at $r_0(0)$ due to secular change of the parameters a_i 's is simply proportional to λ , at lowest order. All coefficients a_4, a_3, a_2, a_1 (the same also holds for a_0 , but a_0 is not present in V_r') are simple linear functions of E, L_z^2 , and Q (c.f. Eq. (37)). Therefore

$$\delta a_i = \int_0^\lambda \frac{da_i}{dt} \frac{dt}{d\lambda'} d\lambda' \quad (99)$$

$$= \int_0^\lambda \left(\frac{\partial a_i}{\partial E} \frac{dE}{dt} + \frac{\partial a_i}{\partial L_z^2} \frac{dL_z^2}{dt} + \frac{\partial a_i}{\partial Q} \frac{dQ}{dt} \right) \frac{dt}{d\lambda'} d\lambda'. \quad (100)$$

On the other hand, each one of these time derivatives of the integrals of motion are exactly equal to 0 when there is no self-force (that is at the limit $\epsilon \rightarrow 0$). However, the derivatives $dE/dt, dL_z^2/dt, dQ/dt$ are not vanishing when a self-force is present. For example

$$\frac{dE}{dt} = \frac{\partial E}{\partial r} \dot{r} + \frac{\partial E}{\partial \eta} \dot{\eta} + \frac{\partial E}{\partial \dot{r}} \ddot{r} + \frac{\partial E}{\partial \dot{\eta}} \ddot{\eta} + \frac{\partial E}{\partial \ddot{\phi}} \ddot{\phi}, \quad (101)$$

since E (as well as Q and L_z^2) is a function of either all $r, \eta, \dot{r}, \dot{\eta}, \ddot{\phi}$, or a few of those. In the expression above, η is simply an abbreviation for $\cos \theta$. The dependence of the expression above, for dE/dt , on the self-force is hidden only in the double time derivatives $\ddot{r}, \ddot{\eta}, \ddot{\phi}$. All other terms, including that part of the double derivatives corresponding to no self-force, have a vanishing net result, since E is an integral of motion for pure gravitational force (geodesic motion), without any extra self-force. Thus

$$\frac{dE}{dt} = \epsilon \left(\frac{\partial E}{\partial \dot{r}} F_r^{(SF)} + \frac{\partial E}{\partial \dot{\eta}} F_\eta^{(SF)} + \frac{\partial E}{\partial \ddot{\phi}} F_\phi^{(SF)} \right). \quad (102)$$

Actually all integrals of motion E, L_z^2, Q are bilinear functions of $\dot{r}, \dot{\eta}, \dot{\phi}$, therefore $\partial E/\partial \dot{r}, \partial E/\partial \dot{\eta}$, and $\partial E/\partial \dot{\phi}$ are simply linear functions of $\dot{r}, \dot{\eta}$, and $\dot{\phi}$, respectively. Thus, collecting all these partial results we end up with a general expression for all a_i 's:

$$\delta a_i = \epsilon \sum_k \int_0^\lambda F_k^{(SF)} \left(\frac{\partial a_i}{\partial E} G_{E,k} + \frac{\partial a_i}{\partial L_z^2} G_{L_z^2,k} + \frac{\partial a_i}{\partial Q} G_{Q,k} \right) \frac{dt}{d\lambda'} d\lambda', \quad (103)$$

where x_k denote the coordinates r, η, ϕ for $k = 1, 2, 3$, respectively, while $G_{E,k} = \partial E/\partial \dot{x}_k$ (and similarly for $G_{L_z^2,k}, G_{Q,k}$) which are linear with respect to \dot{x}_k . Note that all quantities inside the integral should be computed along a geodesic orbit, since δa_i itself is of order ϵ , whereas any deviation from geodesic will cause higher order corrections. Furthermore, assuming that $F_k^{(SF)}$ is of the form $-\dot{x}_k f_k(r, \eta, \dot{x}_l^2)$ —that is, of purely dissipative character—, δa_i will be given by integrals of $(\dot{x}_k)^2$ and other more complicated functions of coordinates r, η and \dot{x}_l^2 . Finally, the term $dt/d\lambda'$ is also a quadratic function of r , and η :

$$\frac{dt}{d\lambda'} = r^2 + a^2 \cos \theta, \quad (104)$$

(see Eq. (166)).

Now, taking into account the almost constant value of r of spherical orbits, the integrand for each δa_i will oscillate, mainly due to η -oscillations, around its average value. Thus all integrals related with δa_i 's (both ω_r^2 and $\delta V_r'(r_0(0), \lambda)$) will consist of a part that scales linearly with λ , due to the average value of the integral, plus an oscillating part, due to η -oscillations. The total λ -time of integration to compute δa_i is assumed sufficiently short to be insensitive to the drift of r -coordinate caused by the self-force, but sufficiently long to span at least a few complete periods of η . Of course, for longer time periods, higher order terms, than the linear terms with respect to λ , will show up. Combining all previous results, Δ will obey the following generic equation:

$$\frac{d^2 \Delta}{d\lambda^2} = - [\omega_0^2 + \epsilon(B\lambda + A_\eta(\lambda))] \Delta - \frac{\epsilon}{e_0} [D\lambda + C_\eta(\lambda) + \dot{r}f_r], \quad (105)$$

where $\omega_0^2 = \omega_r(0)^2$ and

$$B\lambda + A_\eta(\lambda) = \frac{\delta \omega_r^2}{\epsilon}, \quad (106)$$

while

$$D\lambda + C_\eta(\lambda) = \frac{1}{\epsilon} [4\delta a_4 r_0(0)^3 + 3\delta a_3 r_0(0)^2 + 2\delta a_2 r_0(0) + \delta a_1]. \quad (107)$$

The terms $B\lambda, D\lambda$ denote the linear part of the integrals mentioned above, while A_η, C_η denote the oscillating part of the integrals due to η -oscillations of the orbit itself. The last term of the second bracket of the right hand of Eq. (105) is of higher order than the rest terms, since it is proportional to e_0 (the tiny amplitude of the oscillation of r) –the other terms $D\lambda$ and $C_\eta(\lambda)$ are of order unity–, thus it could be omitted. Eq. (105) describes a harmonic oscillator with a drifting frequency, that is driven by an external force which consists of a linear part with respect to time and an oscillating part caused by η oscillations. As a consequence, Δ will oscillate with frequency that varies continuously in an adiabatic fashion, while it slightly oscillates at even harmonics of ω_η (since all functions of η are quadratic with respect to η due to the reflection-symmetry of V_θ). On the other hand, Δ adiabatically drifts away with λ (due to $D\lambda$ term) and is driven by the $C_\eta(\lambda)$ term that oscillates again at even harmonics of η . Especially, if $\omega_r = 2m\omega_\eta$ (where m is some integer), resonance will take place and Δ oscillations will grow in amplitude, until the drift of frequencies (mainly due to the $B\lambda$ term) will bring the system out of resonance. Therefore the mechanical model for the time-dependence of Δ could be described approximately by an equation of the form

$$\frac{d^2\Delta}{dt^2} + [\omega_0^2 + \epsilon_1 t + \epsilon_2 \cos(k\omega_0 t + \phi_1)]\Delta + \epsilon_3 t + \epsilon_4 \cos(k\omega_0 t + \phi_2)] = 0, \quad (108)$$

where $\epsilon_1, \epsilon_2, \epsilon_3, \epsilon_4$ are small numbers, ϕ_1, ϕ_2 are random phases, while k is a factor that regulates resonance or non-resonance condition. The difference in sign of the driving force (the last two terms in the equation above), compared to that of Eq. (105) is deceiving; the D parameter in (105) is negative for a dissipative self force that makes the orbit drift closer to the strong field region. Notice also that the forced oscillator described by Eq. (105) and its simplified model (108) is free of any dissipation, so its amplitude could grow indefinitely, as long as the resonance condition is met –actually the term $\dot{r}f_r$ in Eq. (105), that we omitted in Eq. (108), operates like a dissipative force but of tiny strength.

Finally, we should mention that the oscillatory term $A_\eta(\lambda)$ in Eq. (105) (represented in our harmonic-oscillator model by the term ϵ_2) could in principle lead to parametric resonance as well (when $\Omega_r/(2\Omega_\theta) = m/2$, where m

is an integer). However this is quite difficult to work since the parametric resonance is quite sensitive to the resonance condition.

The similarity between the Kerr problem and the Euler problem is such that the whole process described above fits perfectly well in the analysis of the evolution of spherical orbits in both cases. The Kerr case though does not meet the resonance condition for any kind of spherical orbits as it was suggested in [12] (we did not find any such orbit in Kerr, as well). On the other hand the Euler problem, having small but distinctive quantitative differences from Kerr (the corresponding quartic polynomials of V_r are not identical), does actually admit initial parameters that describe spherical orbits with $\Omega_r = 2\Omega_\theta$. These Eulerian orbits offer an ideal testbed to check our analytic predictions for the evolution of small r -oscillations.

We have actually investigated such oscillations by performing numerical integrations of spherical orbits under an artificial dissipative self-force, of quite arbitrary form. More specifically we have used a self-force of the form

$$\mathbf{F}^{(SF)} = -\epsilon a \frac{1 - \eta^2}{r} \mathbf{v}, \quad (109)$$

where \mathbf{v} is the velocity on oblate spheroidal coordinates (see Appendix A). The form of the self-force has been constructed so as to lead to a loss of energy and angular momentum, while its strength is enhanced at lower r values where the field is stronger, and depends on the η coordinate in a reflection-symmetric way. The components of the self-force on spheroidal coordinates are:

$$F_r^{(SF)} = -\epsilon a \sqrt{\frac{r^2 + a^2 \eta^2}{r^2 + a^2}} \frac{(1 - \eta^2) \dot{r}}{r} \quad (110)$$

$$F_\eta^{(SF)} = -\epsilon a \sqrt{\frac{r^2 + a^2 \eta^2}{1 - \eta^2}} \frac{(1 - \eta^2) \dot{\eta}}{r} \quad (111)$$

$$F_\phi^{(SF)} = -\epsilon a \sqrt{(1 - \eta^2)(r^2 + a^2)} \frac{(1 - \eta^2) \dot{\phi}}{r}, \quad (112)$$

(c.f. Appendix A). We have numerically integrated the time evolution of an Eulerian orbit under the action of the self-force given in the previous paragraph (apart of the gravitational force). The strength parameter ϵ was adjusted to such a low value, ($1/1000$), that the orbit does not deviate significantly from the corresponding geodesic orbit for a time period equivalent to

a few times the maximum period of all orbital frequencies. The initial conditions of the orbit was prepared to obtain a spherical orbit when the self-force was absent. Furthermore different initial conditions were constructed so that the orbit was either at resonance ($\Omega_r = 2\Omega_\theta$), or not. What we have observed in our numerical experiments is that when the almost spherical orbit does not satisfy the resonance condition, the effect of the above self-force is simply a continuous drift of the radius of the orbit towards closer (lower r values) spherical orbits, without any apparent increase in its eccentricity (see Figure 12(b)). However, if the initial spherical orbit meets the resonance condition, there is a noticeable increase in its eccentricity (see Figure 12(a)), while the average r coordinate of the orbit drifts to lower values due to the dissipative self-force. The increase of eccentricity though is not monotonic. At some point, it starts decreasing, like a beating effect. Obviously the resonance condition is then lost and the amplitude of r -oscillations starts decreasing. It should be noted here that although the initial conditions we considered were describing a perfect spherical geodesic orbit, when the self-force were absent, the appearance of an extra self-force is destroying its integrability, and some kind of initial eccentricity was then indirectly induced in the orbit. This tiny eccentricity could either increase (due to resonance) or remain small during the evolution of the orbit when the orbital characteristics keep it out of resonance.

In order to show the relevance of our mathematical model, described by Eq. (108), of a simple driven and drifting harmonic oscillator, we have numerically solved Eq. (108) with parameters: $\omega_0 = 4$, $\epsilon_1 = 0.021$, $\epsilon_2 = 0.01$, $\epsilon_3 = 0.011$, $\epsilon_4 = 0.04$, $\phi_1 = \phi_2 = 0$, and k either 1, which signifies resonance, or 0.6, which describes a non-resonance condition. The evolution of Δ , with initial conditions $\Delta(0) = \dot{\Delta}(0) = 0$, is shown in Figure 13. The evolutionary behavior of Δ looks like what we got in the resonant (or non-resonant) forced Eulerian orbit. We tried to excite parametric resonance in our mathematical model, as well, by choosing $k = 1/2$, but we found that we do need extremely high, non-physical, values of ϵ_2 to achieve this goal. Therefore the oscillating part $A_\eta(\lambda)$ in Eq. (105) seems rather unimportant.

Before ending this section we should note once again the differences between the two times: the Mino-type time parameter λ and the normal time parameter t . With respect to λ both the r oscillations and the η oscillations are periodic with frequency ω_r and ω_η respectively. The corresponding oscillations with respect to t -time are not in general periodic. The fundamental frequencies are in this case Ω_r and Ω_θ . The two types of frequencies are not

equal, but the ratio between them is the same, that is

$$\frac{\Omega_r}{\Omega_\theta} = \frac{\omega_r}{\omega_\eta}, \quad (113)$$

since the ω 's frequencies (with respect to λ) are simply the Y_i components used in the construction of the fundamental frequencies (c.f. Eqs. (169, 170, 174) in Appendix E).

7 Conclusion - Discussion

In this article we have studied thoroughly a Newtonian gravitational field that shares a lot of similarities with the relativistic gravitational field of a Kerr black hole. The fundamental property of both problems that makes them look similar is the fact that both are integrable and separable problems, characterized by three constants of motion, the physical meaning of which is completely analogous in the two cases. These three integrals of motion are the energy, the z -component of the angular momentum, and the Carter constant, a quantity that is quadratic with respect to momenta which could be viewed as a continuous transformation of the square of the total angular momentum of the corresponding spherically symmetric fields (monopole Newtonian and Schwarzschild) when the extra parameter a is introduced so as to destroy the spherical symmetry while retaining the integrability in the two problems. It is quite intriguing that this a parameter has a completely different origin in these two problems: while it represents the spin parameter in Kerr case, it is simply a length in the Euler problem, that defines an imaginary distance between the two half masses governing the axi-symmetric gravitational field. Of course the different physical frame assumed when one studies each problem (the relativistic frame in the former one and the Newtonian in the latter one) introduces restrictions in considering the two problems as completely analogous. For example the horizons in Kerr are absolutely absent in the Euler problem since they are of completely relativistic origin. Also the consideration of space-time as a dynamic entity in the Kerr field leads to the dragging of frames, which has no analogue in the Newtonian frozen space of the Euler problem.

We have attempted to give a complete list of properties of the two problems that are qualitatively (and sometimes quantitatively) comparable, taking into account their intrinsic differences. In some parts of our comparison

we found a way to bridge these differences; the frame-dragging effect has been artificially neutralized, by considering the rotational frequency of a test body with respect to a ZAMO observer as a physical tool to construct equivalent prograde and retrograde orbits in Kerr, so that the physical characteristics of each such pair could be compared, on equal footing, with the omni-directional orbits in the Euler potential. With respect to other fundamental differences, like the existence of horizons in Kerr, we have avoided to approach such regions by considering only orbits that are bound in a fixed region of the gravitational field in both problems without reaching either the plunging region of the Kerr field, or the interior allowed region of the Euler field. Schematically, we have named the orbits that either move exclusively in the interior region or in a region that has been produced by a merge of the two regions of the Euler field, “plunging” or “effectively plunging”, as well).

The similarities between the two problems are summarized in the following list: (i) The separability of the two problems leads to two potentials $V_r(r)$ and $V_\theta(\theta)$ that describe the orbital dynamics. Both share a lot of common properties: V_θ 's have exactly the same form in both problems, while V_r 's are described by 4th order polynomials in which the physical constants of motion are introduced in similar but not exactly equal manner (part of the difference is due to the frame-dragging dynamic property of space-time itself which is incorporated in Kerr's potential). (ii) Due to separability, the wave properties in both fields have analogous characteristics, especially the scalar case. (iii) The multipolar structure of the Euler field is exactly that of Euler, if the current-moments of Kerr are neglected. This makes the two problems behave exactly like each other at least at large distances. (iv) The bound orbits are precessing orbits that move in and out radially. (v) There is an ISCO for both problems. This is of great astrophysical interest since one could describe disks of matter with a finite internal radius. (vi) Although the $a = 0$ case of the Euler problem is the monopole gravitational field leading to simple closed elliptical orbits, whatever the initial conditions are, the $a \rightarrow 0$ Eulerian problem has an ISCO and bound orbits that are not closed in the strong field region, which is also true in the Schwarzschild case. (vi) The bound orbits are characterized by a set of three fundamental frequencies in both problems. The expressions for the frequencies could be written in similar forms, in terms of elliptical integrals, for both problems. Especially in the strong field regime analogous characteristics arise. Thus in a specific region of orbital characteristics, both problems have pairs of distinct orbits with the same set of fundamental frequencies.

A simple first exploitation of this unique analogy between the two problems is to consider the Boyer-Lindquist coordinates that are usually used to describe the Kerr metric not as the analogous of spherical coordinates (used in the Schwarzschild case) but rather as some kind of oblate spheroidal coordinates that are suitably adjusted by the spin parameter a of the Kerr black hole, which is directly related with the quadrupole moment of the black hole itself. This different view-point elucidates the difference in radial proper distance across the equator and across the axis of symmetry of the Kerr metric.

Also, taking into account all the above similarities, one could use the Newtonian problem as a simple mechanical model to discuss and clarify some subtle issues regarding the dynamics of orbits in a Kerr black-hole field. In this article we have reexamined the old argument according to which the “circular” orbits evolve into circular orbits in Kerr, under the action of a self-force arising from the radiation reaction of EMRIs. The evolution of a “spherical” (as we call it here) orbit in the Euler problem under a generic dissipative self-force has been investigated. We have analyzed the dynamic evolution of radial oscillations under the influence of such an external force and ended up into a simple harmonic oscillator toy-model with a drifting and oscillating frequency driven by a force that is partly linear with respect to time and partly oscillating. Both oscillating parts in this mechanical model have the frequency of η^2 , that is twice the Ω_θ frequency and higher even harmonics. According to our toy-model the radial oscillations will grow, mainly due to simple resonance when the resonance condition $\Omega_r = 2k\Omega_\theta$ (with k integer) is met. As explained in Section 6 the parametric resonance (corresponding to $k = 1/2, 1, 3/2, \dots$), although in principle capable to increase exponentially the eccentricity of the orbit, it is quite sensitive to the resonance condition; consequently it is rather difficult to arise when all frequencies are drifting. On the other hand the simple resonance condition (which is met when $k = 1, 2, \dots$) will make the eccentricity grow linearly with time or it will cause a beating effect when the resonance condition is turned on and off due to frequency drift. This analysis could be used to analyze and explain the adiabatic evolution of a spherical orbit either in Kerr or in Euler under any type of perturbative dissipative external force. While in Kerr the fundamental resonance condition has not been found to hold for any kind of spherical orbits, this is not true for the Euler problem. The small quantitative differences between the two problems render the Euler problem suitable to test our model. Having the analytical tools to seek an orbit in the frequency parameter space with suitable frequencies in resonance, it was

quite easy to find such an orbit with $\Omega_r = 2\Omega_\theta$ initially. Then we numerically evolved it under a small external (non-gravitational) dissipative force of very simple form. We actually confirmed that our mathematical model captures the exact qualitative behavior of the orbital eccentricity.

We believe that the analogy presented in this paper could be further used to study the adiabatic passage of an orbit around a black hole through a resonance due to gravitational radiation. The Euler analogue is a perfect tool, we believe, to thoroughly study such a delicate issue that might have implications in the corresponding signal either in the Kerr case (an exact integrable system), or that of a modified slightly non-integrable system (e.g. a perturbed Kerr black hole) by employing, accordingly, a suitable Newtonian analogue of a modified Euler gravitating system that is constructed to be slightly non-integrable. We plan to address these issues in a following paper.

Acknowledgements

TA would like to thank a lot of people with whom he had long discussions, during the past years, about this problem. Katerina Chatziioannou, and later George Pappas were the first persons who performed the first computations regarding some of the similarities relating the orbital characteristics in Euler and in Kerr. Also Charalampos Markakis who shared with us his ideas with respect to generalizations of the notion of Carter constant. Later Kostas Glampedakis collaborated with TA to investigate the similarities at the level of wave properties. Technical advice from Maarten van de Meent's who has acquired a deep intuition on Kerr's resonances was of great help as well. We offer our thanks also to Georgios Lukes-Gerakopoulos for sharing his insightful ideas regarding chaotic behavior of orbits in non-integrable systems with us. AE would like to thank the research funding program I.K.Y. (MIS-5003404) for its support, which was of great importance for the completion of this research project.

A Oblate Spheroidal coordinates

The Lagrangian in oblate spheroidal coordinates (r, η, ϕ) is:

$$L = \frac{1}{2}(r^2 + a^2\eta^2) \left(\frac{\dot{r}^2}{r^2 + a^2} + \frac{\dot{\eta}^2}{1 - \eta^2} \right) + \frac{1}{2}(r^2 + a^2)(1 - \eta^2)\dot{\phi}^2 + \frac{Mr}{r^2 + a^2\eta^2} \quad (114)$$

where $r = a\xi$ (ξ is the radial oblate spheroidal coordinate). An overdot denotes differentiation with respect to time coordinate t .

From Euler-Lagrange equations, we derive the equations of motion:

$$\ddot{r} = \frac{r}{r^2 + a^2\eta^2} \left(-\frac{a^2\dot{r}^2(1 - \eta^2)}{r^2 + a^2} + \frac{\dot{\eta}^2(r^2 + a^2)}{1 - \eta^2} \right) - \frac{2a^2\eta\dot{\eta}\dot{r}}{r^2 + a^2\eta^2} + \frac{r(r^2 + a^2)(1 - \eta^2)\dot{\phi}^2}{r^2 + a^2\eta^2} - \frac{M(r^2 - a^2\eta^2)(r^2 + a^2)}{(r^2 + a^2\eta^2)^3}, \quad (115)$$

$$\ddot{\eta} = -\frac{\eta}{r^2 + a^2\eta^2} \left(-\frac{a^2\dot{r}^2(1 - \eta^2)}{r^2 + a^2} + \frac{\dot{\eta}^2(r^2 + a^2)}{1 - \eta^2} \right) - \frac{2r\dot{r}\dot{\eta}}{r^2 + a^2} - \frac{\eta(r^2 + a^2)(1 - \eta^2)\dot{\phi}^2}{a^2 + r^2\eta^2} - \frac{2Ma^2r\eta(1 - \eta^2)}{(r^2 + a^2\eta^2)^3}, \quad (116)$$

$$\ddot{\phi} = \left(-\frac{2r\dot{r}}{r^2 + a^2} + \frac{2\eta\dot{\eta}}{1 - \eta^2} \right) \dot{\phi}. \quad (117)$$

We used the above equations for integrating numerically the orbits and not Eqs. (34)-(36). When the latter ones were used in a numerical integration scheme, Eqs. (34)-(36) accumulate error at the turning points due to the square roots. Moreover the signs of the r and θ velocities have to be changed every time the orbit passes through a turning point.

The oblate spheroidal unit vectors are [29]:

$$\begin{aligned} \hat{\mathbf{r}} &= r\sqrt{\frac{1 - \eta^2}{r^2 + a^2\eta^2}} \cos \phi \hat{\mathbf{i}} + r\sqrt{\frac{1 - \eta^2}{r^2 + a^2\eta^2}} \sin \phi \hat{\mathbf{j}} + \eta\sqrt{\frac{r^2 + a^2}{r^2 + a^2\eta^2}} \hat{\mathbf{k}} \\ \hat{\boldsymbol{\eta}} &= -\eta\sqrt{\frac{r^2 + a^2}{r^2 + a^2\eta^2}} \cos \phi \hat{\mathbf{i}} - \eta\sqrt{\frac{r^2 + a^2}{r^2 + a^2\eta^2}} \sin \phi \hat{\mathbf{j}} + r\sqrt{\frac{1 - \eta^2}{r^2 + a^2\eta^2}} \hat{\mathbf{k}} \\ \hat{\boldsymbol{\phi}} &= -\sin \phi \hat{\mathbf{i}} + \cos \phi \hat{\mathbf{j}}, \end{aligned}$$

where $(\hat{\mathbf{i}}, \hat{\mathbf{j}}, \hat{\mathbf{k}})$ are the Cartesian unit vectors. Finally the position vector \mathbf{r} is:

$$\mathbf{r} = r \sqrt{\frac{r^2 + a^2}{r^2 + a^2 \eta^2}} \hat{\mathbf{r}} - a^2 \eta \sqrt{\frac{1 - \eta^2}{r^2 + a^2 \eta^2}} \hat{\boldsymbol{\eta}}, \quad (118)$$

while the velocity vector $\mathbf{v} = d\mathbf{r}/dt$ expressed in terms of oblate spheroidal coordinates is:

$$\mathbf{v} = \dot{r} \sqrt{\frac{r^2 + a^2 \eta^2}{r^2 + a^2}} \hat{\mathbf{r}} + \dot{\eta} \sqrt{\frac{r^2 + a^2 \eta^2}{1 - \eta^2}} \hat{\boldsymbol{\eta}} + \dot{\phi} \sqrt{(r^2 + a^2)(1 - \eta^2)} \hat{\boldsymbol{\phi}}. \quad (119)$$

B Parameterization of orbits

The potentials $V_r(r)$ of Eq. (37) and V_θ of Eq. (38), that govern the bound motion, could be rewritten as:

$$V_r(r) = 2E(r - r_1)(r - r_2)(r - r_3)(r - r_4), \quad (120)$$

$$V_\theta(\theta) = \frac{-2a^2 E}{1 - \cos^2 \theta} (z_- - \cos^2 \theta)(z_+ - \cos^2 \theta). \quad (121)$$

Note the E here is the initial Eulerian energy before, its substitution by the corresponding relativistic analogue. The radial potential has either four real roots with order $r_4 \leq r_3 \leq r_2 \leq r_1$ or two real roots with order $r_2 \leq r_1$ and two complex conjugate roots r_3, r_4 . The roots of longitudinal potential are $\pm\sqrt{z_-}, \pm\sqrt{z_+}$ which satisfy the inequalities $z_- \leq 1$ and $z_+ > 1$. Normal bound orbits have $r_2 \leq r \leq r_1$ and $-\sqrt{z_-} \leq \cos \theta \leq \sqrt{z_-} = \cos \theta_{\min}$. We have excluded from our study bound orbits with $r_4 \leq r \leq r_3$ (considering them plunging orbits), while z_+ does not correspond to any physical θ value.

At numerical calculation we have used the orbital parameters $\{e, p, \theta_{\min}\}$ as a useful parametrization of bound orbits. Where $e = (r_1 - r_2)/(r_1 + r_2)$ is the eccentricity, $p = 2r_1 r_2/(r_1 + r_2)$ is the semi-latus rectum and θ_{\min} is the lowest polar angle along the orbit. The turning points of a normal bound orbit become:

$$r_1 = \frac{p}{1 - e} \quad , \quad r_2 = \frac{p}{1 + e} \quad , \quad z_- = \cos^2 \theta_{\min}. \quad (122)$$

The rest of the roots of the potentials (120) and (121) can be computed from the form of the polynomials and the corresponding constants of motion

$\{E, L_z, Q\}$. Analyzing (120) and equating to (37) we obtain the following equations:

$$\begin{aligned} -2E(r_1 + r_2 + r_3 + r_4) &= 2M, \\ 2Er_1r_2r_3r_4 &= -Qa^2, \end{aligned}$$

which end up to the following expressions:

$$r_3 = \frac{A + \sqrt{A^2 - 4B}}{2}, \quad r_4 = \frac{B}{r_3}, \quad (123)$$

where

$$A = -\frac{M}{E} - (r_1 + r_2) \quad (124)$$

and

$$B = \frac{a^2Q}{-2Er_1r_2}. \quad (125)$$

Also, equating (38) and (121) we find:

$$-2a^2Ez_-z_+ = Q$$

which gives:

$$z_+ = \frac{Q}{-2a^2Ez_-}. \quad (126)$$

Next we need to express the constants of motion $\{E, L_z, Q\}$, showing up in the expressions above, in terms of the orbital parameters $\{p, e, \theta_{\min}\}$. For the Kerr space-time, similar expressions have been given by Schmidt in Appendix B of [25]. We use the condition of turning points ($d\theta/dt = 0$) at $\theta = \theta_{\min}$ to express Q as a function of (E, L_z, z_-) :

$$Q = z_- \left[-2a^2E + \frac{L_z^2}{1 - z_-} \right], \quad (127)$$

and rewrite the radial potential as:

$$V_r(r) = 2Ef(r) - L_z^2g(r) + d(r), \quad (128)$$

where the functions:

$$\begin{aligned} f(r) &= r^4 + a^2(1 + z_-)r^2 + a^4z_-, \\ g(r) &= \frac{r^2 + a^2z_-}{1 - z_-}, \\ d(r) &= 2Mr^3 + 2Ma^2r. \end{aligned}$$

Furthermore we impose $dr/dt = 0$ at r_1 and r_2 . (For circular orbits with $r_1 = r_2 = r_0$ we should solve simultaneously the equations $dr/dt = 0$ and $d^2r/dt^2 = 0$ at r_0 .) The energy E and angular momentum L_z are then given by:

$$E = -\frac{\kappa}{2\rho}, \quad (129)$$

$$L_z = \pm\left(\frac{\tau}{\rho}\right)^{1/2}, \quad (130)$$

where the determinants ρ, κ, τ are defined as:

$$\rho = f_1 g_2 - f_2 g_1, \quad (131)$$

$$\kappa = d_1 g_2 - d_2 g_1, \quad (132)$$

$$\tau = f_1 d_2 - f_2 d_1. \quad (133)$$

In the above expressions for the determinants the subscripts 1, 2 have the following meaning:

i. for eccentric orbits ($e \neq 0$):

$$(f_1, g_1, d_1) = (f(r_1), g(r_1), d(r_1)), \quad (134)$$

$$(f_2, g_2, d_2) = (f(r_2), g(r_2), d(r_2)), \quad (135)$$

ii. for circular orbits ($e = 0$ and $r_1 = r_2 = r_0$):

$$(f_1, g_1, d_1) = (f(r_0), g(r_0), d(r_0)), \quad (136)$$

$$(f_2, g_2, d_2) = (f'(r_0), g'(r_0), d'(r_0)). \quad (137)$$

In total, starting from the three orbital parameters $\{e, p, \theta_{\min}\}$: (a) we construct the determinants ρ, κ, τ , using Eqs. (131-133), (b) from them we compute the constants of motion E, L_z and Q through Eqs. (129, 130, 127), and (c) we finally obtain the four radial roots of V_r (from Eq. (123)) and the second root, z_+ , of V_θ (from Eq. (126)).

C Separatrix

The separatrix describes all orbits that are essentially circular although their eccentricity is not necessarily zero. It is defined as the set of orbits with

$r_2 = r_3$. Due to this double root the orbit spends infinite time to approach this root, therefore it evolves into an eternally circular orbit.

In this Appendix we parametrize these orbits by two parameters e (the eccentricity) and $x = r_4/r_3$. From these two parameters we will show that one could construct the rest orbital parameters (p, z_-) , as well as the constants of motion E, L_z, Q . We will show also that the new parameter x is intimately related to the inclination of the orbit. Thus for $x = 0$ the orbit is equatorial ($\theta_{\min} = \pi/2$), while for $x = 1$ we get the maximally inclined orbit ($\theta_{\min} = \min$).

Let's start from the radial potential (37):

$$V_r(r) = 2Er^4 + 2Mr^3 + (2Ea^2 - Q - L_z^2)r^2 + 2Ma^2r - Qa^2 \quad (138)$$

which is a polynomial of degree four:

$$\begin{aligned} P_4(r) &= 2E(r - r_1)(r - r_2)(r - r_3)(r - r_4) \\ &= 2E[r^4 - (r_1 + r_2 + r_3 + r_4)r^3 \\ &\quad + (r_1r_2 + r_1r_3 + r_1r_4 + r_2r_3 + r_2r_4 + r_3r_4)r^2 \\ &\quad - (r_1r_2r_3 + r_1r_2r_4 + r_1r_3r_4 + r_2r_3r_4)r + r_1r_2r_3r_4], \end{aligned} \quad (139)$$

where the roots r_1, r_2, r_3, r_4 are given in Appendix B. The motion of a particle is restricted between $r_2 \leq r \leq r_1$ (Section 3.2). On separatrix, $r_2 = r_3 = p/(1 + e)$. The smallest root r_4 , always lies within the interval $[0, r_3]$ thus $r_4 = xr_3 = xp/(1 + e)$, where $x \in [0, 1]$. Equating the coefficients of the polynomials (138), and (139) and introducing the above parametrization for r_1, r_2, r_3, r_4 we derive the following set of equations:

$$2M = -2EMp \frac{(3 - e) + x(1 - e)}{1 - e^2}, \quad (140)$$

$$2Ea^2 - Q - L_z^2 = 2E \frac{M^2 p^2}{(1 + e)^2(1 - e)} ((3 + e) + x(3 - e)), \quad (141)$$

$$2Ma^2 = -2E \frac{M^3 p^3}{(1 + e)^3(1 - e)} ((1 + e) + x(3 + e)), \quad (142)$$

$$-Qa^2 = \frac{2EM^4 p^4 x}{(1 - e)(1 + e)^3}. \quad (143)$$

Solving this system of equations we can express the constants of motion and the semi-latus rectum as functions with respect to the eccentricity e and the

parameter x only:

$$p(e, x) = \frac{a}{M}(1+e)\sqrt{\frac{3-e+x(1-e)}{1+e+x(3+e)}}, \quad (144)$$

$$E(e, x) = -\frac{(1-e)M}{a}\sqrt{\frac{1+e+x(3+e)}{(3-e+x(1-e))^3}}, \quad (145)$$

$$Q(e, x) = 2Ma(1+e)x\sqrt{\frac{3-e+x(1-e)}{(1+e+x(3+e))^3}}, \quad (146)$$

$$L_z^2(e, x) = 16Ma\sqrt{\frac{1+e+x(3+e)}{(3-e+x(1-e))^3}} \times \frac{(1+x)^2[1+x+e(1-x)]}{(1+e+x(3+e))^2}. \quad (147)$$

The $z_- = \cos^2 \theta_{\min}$ is the lower root of the quadratic equation $V_\theta(\theta) = 0$. That is:

$$z_- = \frac{C - \sqrt{C^2 + 8a^2EQ}}{-4a^2E}, \quad (148)$$

where $C = Q + L_z^2 - 2a^2E$. Replacing (144)-(147) in (148), we obtain:

$$z_-(e, x) = \frac{3-e+x(1-e)}{2(1-e)(1+e+x(3+e))} \times \left[3+e+x(3-e) - \sqrt{(3+e+x(3-e))^2 - 4x(1-e^2)} \right]. \quad (149)$$

For a fixed eccentricity e , $z_-(e, x)$ is a monotonically increasing function of x . It takes its greatest value at $x = 1$, while for $x = 0$, it is $z_-(e, 0) = 0$ (equatorial orbits), as mentioned earlier. This parameter x is not very practical for bound orbits in Kerr, though, since the maximally inclined orbits in Kerr do not correspond to $x = 1$.

D Fundamental Frequencies

In this Appendix we give analytic expressions that one could use to calculate the fundamental frequencies of normal bound orbits in the Euler field. We will exploit the action-angle variables formalism [10]. We denote the constants of motion as: $F_i = (H = E, L_z, Q)$. The canonical momenta are:

$p_\phi = L_z$, $p_r = \sqrt{V_r(r)}/(r^2 + a^2)$ and $p_\theta = \sqrt{V_\theta(\theta)}$, with the potentials given in Eqs. (37) and (38). The definition of the action variables, of Eq. (67), give:

$$J_r = \frac{1}{2\pi} \oint \frac{\sqrt{V_r(r)}}{r^2 + a^2} dr, \quad (150)$$

$$J_\theta = \frac{1}{2\pi} \oint \sqrt{V_\theta} d\theta, \quad (151)$$

$$J_\phi = \frac{1}{2\pi} \oint p_\phi d\phi = L_z. \quad (152)$$

In order to derive the corresponding frequencies

$$\Omega_i(\mathbf{J}) = \frac{\partial H(\mathbf{J})}{\partial J_i},$$

we should first express the Hamiltonian with respect to the action variables $H(\mathbf{J})$, which can't be done analytically. The integrals (150)-(152) of action variables, cannot be explicitly inverted. However, we can calculate the frequencies from the inverse derivatives $\partial J_i / \partial F_j$, combined with the chain rule. The non trivial partial derivatives are:

$$\frac{\partial J_r}{\partial H} = \frac{Y}{\pi} \quad (153)$$

$$\frac{\partial J_r}{\partial L_z} = -\frac{Z}{\pi} \quad (154)$$

$$\frac{\partial J_r}{\partial Q} = -\frac{X}{2\pi} \quad (155)$$

$$\frac{\partial J_\theta}{\partial H} = \frac{2a^2 \sqrt{z_+}}{\pi\beta} (K(k) - E(k)) \quad (156)$$

$$\frac{\partial J_\theta}{\partial L_z} = \frac{2L_z}{\pi\beta \sqrt{z_+}} (K(k) - \Pi(z_-, k)) \quad (157)$$

$$\frac{\partial J_\theta}{\partial Q} = \frac{1}{\pi\beta \sqrt{z_+}} K(k) \quad (158)$$

with $K(k)$, $E(k)$ and $\Pi(z_-, k)$ being the 1st, 2nd and 3rd complete elliptic integrals that are given in Eqs. (77, 78, 79), while the quantities Y , Z and

X are the radial integrals:

$$Y = \int_{r_1}^{r_2} \frac{r^2}{\sqrt{V_r}} dr, \quad (159)$$

$$Z = \int_{r_1}^{r_2} \frac{L_z r^2}{(r^2 + a^2) \sqrt{V_r}} dr \quad (160)$$

$$X = \int_{r_1}^{r_2} \frac{dr}{\sqrt{V_r}}. \quad (161)$$

Finally the two extra quantities β, k shown above are defined as $\beta^2 = -2a^2 E$ and $k^2 = z_-/z_+$. Now we can inverse the derivatives (153)-(158), using the chain rule

$$\frac{\partial F_i}{\partial J_j} \frac{\partial J_j}{\partial F_k} = \delta_k^i. \quad (162)$$

By setting $F_i = H$ we obtain the system of equations:

$$\begin{aligned} \frac{\partial H}{\partial J_r} \frac{\partial J_r}{\partial H} + \frac{\partial H}{\partial J_\theta} \frac{\partial J_\theta}{\partial H} &= 1 \\ \frac{\partial H}{\partial J_r} \frac{\partial J_r}{\partial L_z} + \frac{\partial H}{\partial J_\theta} \frac{\partial J_\theta}{\partial L_z} + \frac{\partial H}{\partial J_\phi} \frac{\partial J_\phi}{\partial L_z} &= 0 \\ \frac{\partial H}{\partial J_r} \frac{\partial J_r}{\partial Q} + \frac{\partial H}{\partial J_\theta} \frac{\partial J_\theta}{\partial Q} &= 0. \end{aligned}$$

which solved with respect to $\partial H / \partial J_i$ provides us with the desired frequencies:

$$\Omega_r = \frac{\pi K(k)}{a^2 z_+ [K(k) - E(k)] X + Y K(k)}, \quad (163)$$

$$\Omega_\theta = \frac{\pi \beta \sqrt{z_+} X / 2}{a^2 z_+ [K(k) - E(k)] X + Y K(k)}, \quad (164)$$

$$\Omega_\phi = \frac{Z K(k) + X L_z [\Pi(z_-, k) - K(k)]}{a^2 z_+ [K(k) - E(k)] X + Y K(k)}. \quad (165)$$

Although the denominators of the integrals (159, 161) vanish when the orbit passes through a turning point, *Mathematica* is capable to compute the above frequencies. We should note that the above expressions for the fundamental frequencies are identical to those for Kerr orbits (c.f. [25]), except of the actual form of V_r and the form of the integral Z .

E Alternative analytical expressions for the frequencies

We should emphasize the fact that the expressions for the fundamental frequencies derived in Appendix D, directly from the formalism of action-angle variables turn into indefinite expressions when $r_2 \rightarrow r_3$ (separatrix). Then one needs to resort in approximating analytical expressions for this region, which is quite challenging especially for generic orbits. Another major problem is that the r and θ oscillations are not periodic in coordinate time t , since the corresponding equations (c.f. Eqs. (34, 35)) are coupled through the quantity $r^2 + a^2 \cos^2 \theta$. Following [30], in order to decouple the radial and polar motion, we introduce a new time variable,

$$d\lambda = \frac{dt}{r^2 + a^2 \cos^2 \theta}, \quad (166)$$

by analogy with the Mino time, which is widely used in the study of geodesic orbits in Kerr. Then the corresponding variables become strictly periodic with respect to λ . It is preferable to derive new analytical expressions for the frequencies exploiting the elliptic integrals and the new time variable (166) as Fujita and Hikida did for Kerr.

The geodesic equations in the new time variable λ become:

$$\begin{aligned} \left(\frac{dr}{d\lambda} \right)^2 &= V_r(r), \\ \left(\frac{d \cos \theta}{d\lambda} \right)^2 &= \tilde{V}_\theta(\cos \theta), \\ \frac{d\phi}{d\lambda} &= \Phi_r(r) + \Phi_\theta(\cos \theta) - aE, \\ \frac{dt}{d\lambda} &= r^2 + a^2 \cos^2 \theta. \end{aligned} \quad (167)$$

where the new functions $\tilde{V}_\theta, \Phi_r(r), \Phi_\theta$ that are introduced above are:

$$\begin{aligned} \tilde{V}_\theta(\cos \theta) &= V_\theta(\theta)(1 - \cos^2 \theta) = Q - (Q - 2a^2 E + L_z^2) \cos^2 \theta - 2a^2 E \cos^4 \theta, \\ \Phi_r(r) &= a \frac{E(r^2 + a^2) - aL_z}{r^2 + a^2}, \\ \Phi_\theta(\cos \theta) &= \frac{L_z}{1 - \cos^2 \theta}. \end{aligned} \quad (168)$$

The frequency of the r -motion and θ -motion, with respect to λ , will be denoted Y_r and Y_θ , respectively. Similarly, one can define the azimuthal λ -frequency Y_ϕ and the frequency Γ of the coordinate time t with respect to λ . Following the procedure of [30], we derive all λ frequencies for the Euler problem.

The radial (37) and polar (121) potentials are polynomials of order four for both Euler and Kerr, so Y_r and Y_θ of Euler are exactly the same with that of Kerr, when written in terms of the roots of the corresponding polynomial. We will write the final expressions and not reproduce all the calculations here (the various new quantities introduced here will be analytically presented at the end). The process is exactly the same with that for the Kerr field:

$$Y_r = \frac{\pi \sqrt{-2E(r_1 - r_3)(r_2 - r_4)}}{2K(k_r)}, \quad (169)$$

$$Y_\theta = \frac{\pi L_z \sqrt{\epsilon_0 z_+}}{2K(k_\theta)}, \quad (170)$$

while the Y_ϕ and Γ for Kerr are defined by Eqs. (7), (8) of [30]. When they are translated into the Euler case they yield the following form:

$$\Gamma = Y_{t(r)} + Y_{t(\theta)}, \quad (171)$$

$$Y_\phi = Y_{\phi(r)} + Y_{\phi(\theta)} - aE, \quad (172)$$

where:

$$\begin{aligned} Y_{t(r)} &= \langle r^2 \rangle_\lambda \\ Y_{t(\theta)} &= \langle a^2 \cos^2 \theta \rangle_\lambda \\ Y_{\phi(r)} &= \langle \Phi_r(r) \rangle_\lambda \\ Y_{\phi(\theta)} &= \langle \Phi_\theta(\cos \theta) \rangle_\lambda \end{aligned}$$

and $\langle f(x) \rangle_\lambda$ denotes the average over λ . Φ_r could be recast in the following form

$$\Phi_r(r) = \frac{a}{r_+ - r_-} \left(-\frac{aL_z}{r - r_+} + \frac{aL_z}{r - r_-} \right) + aE, \quad (173)$$

and using the expressions and integrals from Appendix A of [30], we obtain the following expressions for the rest frequencies:

$$\begin{aligned}
Y_\phi = & \frac{2Y_\theta}{\pi\sqrt{\epsilon_0 z_+}} \Pi(z_-, k_\theta) + \frac{2aY_r}{\pi(r_+ - r_-) \sqrt{-2E(r_1 - r_3)(r_2 - r_4)}} \times \\
& \left(\frac{-aL_z}{r_3 - r_+} \left[K(k_r) - \frac{r_2 - r_3}{r_2 - r_+} \Pi(h_+, k_r) \right] \right. \\
& \left. + \frac{aL_z}{r_3 - r_-} \left[K(k_r) - \frac{r_2 - r_3}{r_2 - r_-} \Pi(h_-, k_r) \right] \right), \quad (174)
\end{aligned}$$

$$\begin{aligned}
\Gamma = & \frac{2Y_\theta a^2 z_+}{\pi L_z \sqrt{\epsilon_0 z_+}} [K(k_\theta) - E(k_\theta)] \\
& + \frac{Y_r}{\pi \sqrt{-2E(r_1 - r_3)(r_2 - r_4)}} [(r_3(r_1 + r_2 + r_3) - r_1 r_2) K(k_r) \\
& + (r_2 - r_3)(r_1 + r_2 + r_3 + r_4) \Pi(h_r, k_r) + (r_1 - r_3)(r_2 - r_4) E(k_r)]. \quad (175)
\end{aligned}$$

The various quantities that appear on the formulae for the frequencies above are defined as:

$$\epsilon_0 = \frac{-2a^2 E}{L_z^2}, \quad (176)$$

$$k_r = \sqrt{\frac{r_1 - r_2}{r_1 - r_3} \frac{r_3 - r_4}{r_2 - r_4}}, \quad (177)$$

$$k_\theta = \sqrt{\frac{z_-}{z_+}}, \quad (178)$$

$$r_\pm = \pm ia, \quad (179)$$

$$h_\pm = \frac{(r_1 - r_2)(r_3 - r_\pm)}{(r_1 - r_3)(r_2 - r_\pm)}, \quad (180)$$

$$h_r = \frac{r_1 - r_2}{r_1 - r_3}, \quad (181)$$

while the expressions $K(k)$, $E(k)$ and $\Pi(n, k)$ are the complete elliptic integrals of first, second and third kind respectively (note that [30] has different conventions for the elliptic integrals than the ones used in this article).

The fundamental frequencies in coordinate time t are finally given by:

$$\begin{aligned}
\Omega_r &= \frac{Y_r}{\Gamma} \\
\Omega_\theta &= \frac{Y_\theta}{\Gamma} \\
\Omega_\phi &= \frac{Y_\phi}{\Gamma}. \quad (182)
\end{aligned}$$

On the plots of the text all fundamental frequencies of the Euler problem were calculated based on the analytical expressions (182). These formulae are precise and easy to calculate by means of *Mathematica* even for the region close to separatrix that is when $r_2 \rightarrow r_3$.

Especially at the separatrix the expressions for the frequencies are greatly simplified since the ratios between some elliptic integrals vanish, that is,

$$\frac{E(k_r)}{K(k_r)} \xrightarrow{r_3 \rightarrow r_2} 0, \quad (183)$$

and

$$(r_2 - r_3) \frac{\Pi(h_{r,+,-}, k_r)}{K(k_r)} \xrightarrow{r_3 \rightarrow r_2} 0. \quad (184)$$

The final expressions for the frequencies at the separatrix are still given by Eqs. (182), but now the various components Y_i 's and Γ are much simpler:

$$\begin{aligned} Y_r &= 0 \\ Y_\theta &= \frac{\pi L_z \sqrt{\epsilon_0 z_+}}{2K(k_\theta)} \\ Y_\phi &= L_z \left(\frac{\Pi(z_-, k_\theta)}{K(k_\theta)} - \frac{a^2}{r_2^2 + a^2} \right) \\ \Gamma &= a^2 z_+ \left(1 - \frac{E(k_\theta)}{K(k_\theta)} \right) + r_2^2. \end{aligned} \quad (185)$$

References

- [1] L. Euler, Nov. Comm. Acad. Imp. Petropolitanae, **10**, pp. 207-242, **11**, pp. 152-184; Mémoires de l'Acad. de Berlin, **11**, 228-249. 1760.
- [2] E.T. Whittaker, *A Treatise on the Analytical Dynamics of Particles and Rigid Bodies (4th Edition)*, Cambridge Univ. Press, 1989.
- [3] R. P. Kerr, Phys. Rev. Lett. **11**, 237 (1963).
- [4] B. Carter, Phys. Rev. Lett. **26**, 331 (1971).
- [5] S. Chandrasekhar, *The Mathematical Theory of Black Holes*, Oxford Univ. Press, 1983.

- [6] B.P. Abbott et al. (LIGO Scientific Collaboration and Virgo Collaboration), Phys. Rev. Lett. **116**, 061102 (2016), arXiv:gr-qc/1602.03837.
- [7] E. Poisson, A. Pound and I. Vega, Living Rev. Relativity **14**, 7 (2011), arXiv:gr-qc/1102.0529.
- [8] B. Carter, Commun. Math. Phys. **10**, 280 (1968).
- [9] K. Rosquist, T. Bylund and L. Samuelsson, Int. Journal.of Mod. Phys. D **18**, 429 (2009).
- [10] V. I. Arnold, *Mathematical Methods of Classical Mechanics (2nd Edition)*, Springer, New York, 1989.
- [11] C. M. Will, Phys. Rev. Lett. **102**, 061101, (2009).
- [12] D. Kennefick and A. Ori, Phys. Rev. D **53**, 4319 (1996), arXiv:gr-qc/9512018.
- [13] G. Lukes-Gerakopoulos, T. A. Apostolatos and G. Contopoulos, Phys. Rev. D **81**, 124005 (2010), arXiv:gr-qc/1003.3120.
- [14] A. N. Kolmogorov, Dokl. Akad. Nauk SSSR **98**, 527(1954); V. I. Arnold, Russ. Math. Surv. **18**, 13 (1963); J. Moser, Nachr. Akad. Wiss. Göttingen Math.-Phys. Kl. II **1**(1962).
- [15] H. Poincaré, Rend. Circ. Mat. Palermo **33**, 375 (1912); G. D. Birkhoff, Trans. Am. Math. Soc. **14**, 14 (1913).
- [16] L. D. Landau and E. M. Lifshitz, *Mechanics (3rd Edition)*, Butterworth-Heinemann, Oxford, 1976.
- [17] D. Lynden-Bell, MNRAS **338**, 208 (2003).
- [18] W. Israel, Phys. Rev. D **2**, 641 (1970).
- [19] H. Keres, Soviet Phys. JETP **25**, 504 (1967).
- [20] C. Markakis, MNRAS **441**, 2974-2985 (2014), arXiv:gr-qc/1202.5228.
- [21] K. Glampedakis and T.A. Apostolatos, Classical and Quantum Gravity **30**, 055006 (2013), arXiv:gr-qc/1301.3309.

- [22] J.M. Bardeen, W.H. Press and S.A. Teukolsky, *Astrophys. J.* **178**, 347 (1972).
- [23] K. S. Thorne, R. H. Price and D. A. MacDonald, *Black Holes: the Membrane Paradigm*, Yale University Press, 1986.
- [24] M. Abramowitz and I.A. Stegun, *Handbook of Mathematical Functions*, Dover, New York, 1965.
- [25] W. Schmidt, *Classical and Quantum Gravity* **19**, 2743 (2002), arXiv:gr-qc/0202090.
- [26] T. Hinderer and É. É. Flanagan, *Phys. Rev. D* **78**, 064028 (2008), arXiv:gr-qc/0805.3337.
- [27] N. Warburton, L.Barack and N. Sago, *Phys. Rev. D* **87**, 084012 (2013), arXiv:gr-qc/1301.3918.
- [28] F. D. Ryan, *Phys. Rev. D* **52**, R3159 (1995), arXiv:gr-qc/9506023.
- [29] S. X. K. Howusu, F. J. N Omaghali and F. F. Musongong, *Journal of Applied Sciences* Volume **7**, Number 1 2004.
- [30] R. Fujita and W. Hikida, *Classical and Quantum Gravity* **26**, 135002 (2009), arXiv:gr-qc/0906.1420.

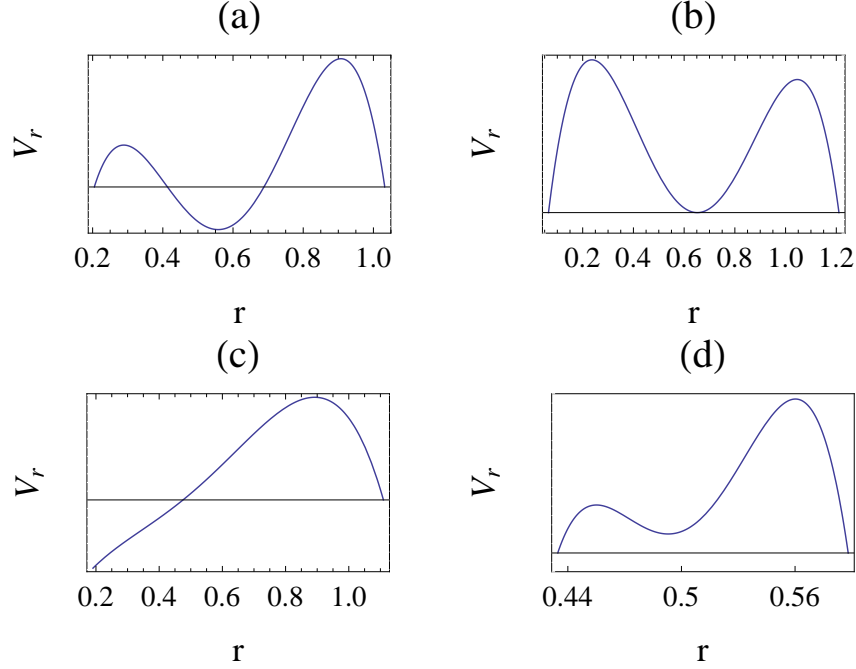


Figure 1: This is a collection of different forms of potentials V_r (by choosing different sets of parameters E, L_z, Q) leading to different types of orbits. The orbit evolves in-between two successive roots of the potential where $V_r > 0$. In plot (a) there are two distinct regions of allowed r 's. The bound orbits we are mostly interested in are orbits in the exterior allowed region (the ones of the interior region are 'plunging orbits'). In plot (b) a marginal case for the potential is depicted. Two of the roots of the potential coincide ($r_2 = r_3$), so the normal bound orbit spends infinite time approaching r_2 . This is a separatrix case which is further discussed in the next Section. Plots (c) and (d) show two cases where two of the roots are complex. The former one is a normal bound orbit without any plunging dual, while in the latter one the two regions of plot (a) have been merged forming an 'effectively plunging orbit'. We will not consider these in our analysis, since their analogue in Kerr refers to a geodesic orbit that eventually plunges under the horizon of the black hole.

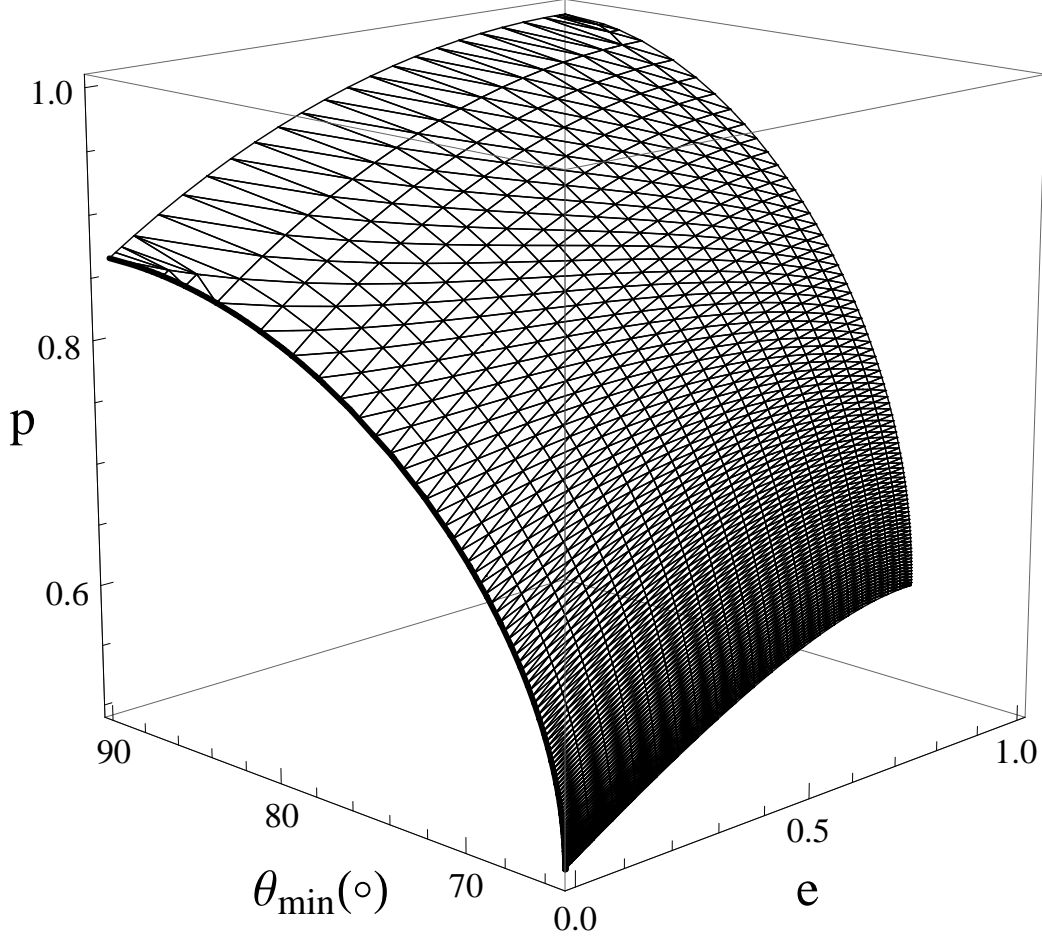


Figure 2: The surface depicts the orbital parameters of the separatrix of the Euler problem in (e, p, θ_{\min}) -space, for $a = 0.5M$. The normal bound orbits we consider lie above this separatrix surface. The thick line (in front) corresponds to spherical ($r = \text{const} = r_1 = r_2 = r_3$) orbits, that is, to orbits with $e = 0$. The upper left corner of the surface at $e = 0, \theta_{\min} = \pi/2$ corresponds to the ISCO. This plots shows clearly that the separatrix extends up to a minimum value of θ_{\min} which is a function of e (the bottom boundary of the surface). It is obvious that there is no separatrix of the Euler problem for orbits that have a large inclination. The semi-latus rectum is measured in units of M .

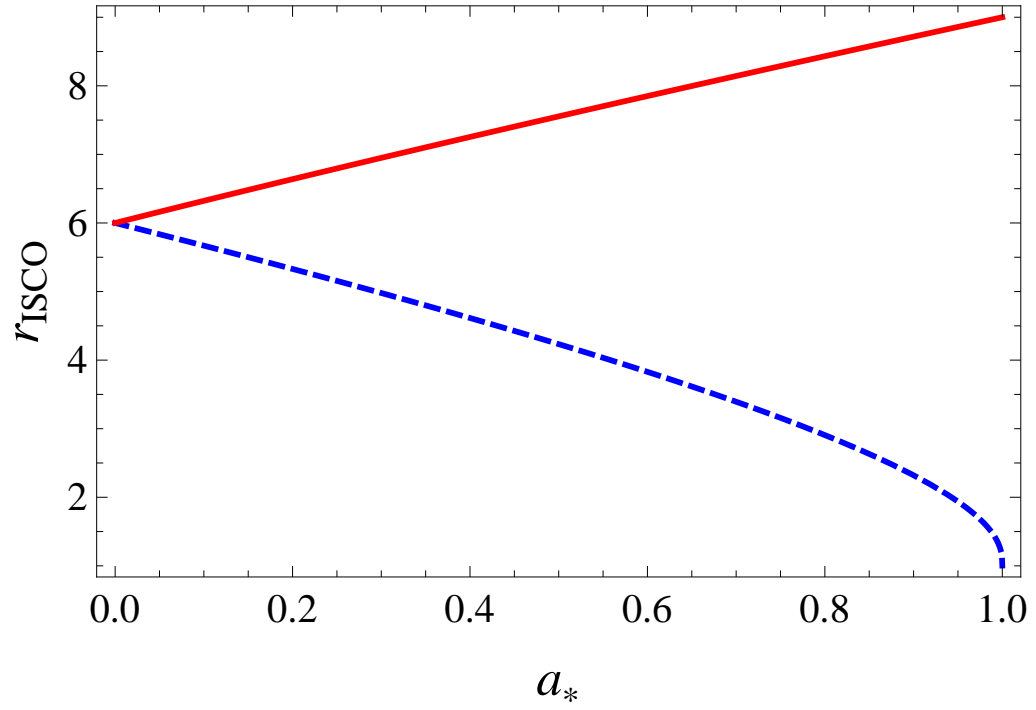


Figure 3: This is the plot of r_{ISCO} as a function of a_* for prograde (blue dashed curve) and for retrograde (red curve) orbits in Kerr, according to Eq. (59). The radii are scaled with M .

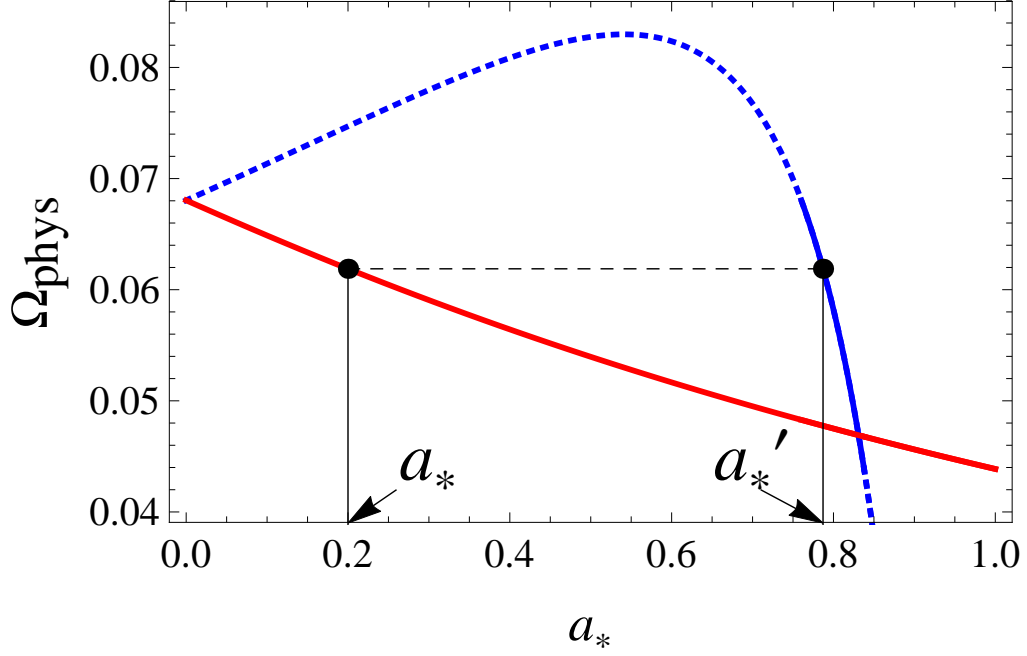


Figure 4: This is the plot of the absolute value of Ω_{phys} , described in the text, at r_{ISCO} as a function of a_* for prograde (blue dotted and solid curve) and for retrograde (red curve) orbits. In order to form pairs of ISCO counter-rotating orbits with equal values of Ω_{phys} (like the pair of black dots) we assign the value of a_* of the retrograde orbit to the prograde orbit corresponding to a different actual a_*' but with equal Ω_{phys} . The two parts of the blue curve (prograde orbits) with no corresponding retrograde dual have been plotted as blue dotted curves. Only the solid part of this curve have an Ω_{phys} that is equal to the corresponding value of a retrograde orbit. The average radius $\langle r_{\text{ISCO}} \rangle$ of the two radii for each such pair is considered the ISCO radius corresponding to the particular a_* value.

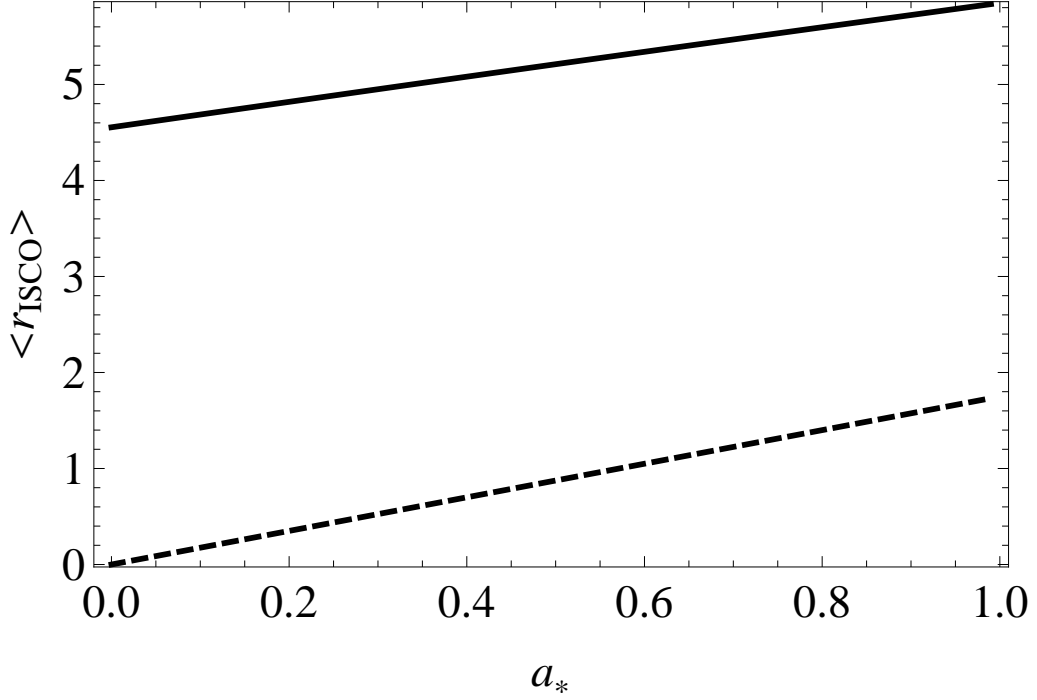


Figure 5: The solid curve shows the dependence of $\langle r_{\text{ISCO}} \rangle$, which is defined in Eq. (62), as a function of a_\star . Although it is apparently linear, this is not exactly true. The dashed curve shows the dependence of r_{ISCO} on a_\star for the Euler problem. The oppositely directed orbits in the latter case have equal radii. The two lines have somewhat different slopes (the average slope of the almost linear curve corresponding to Kerr is ~ 1.3 , while the exactly straight line for Euler has slope $\sqrt{3}$).

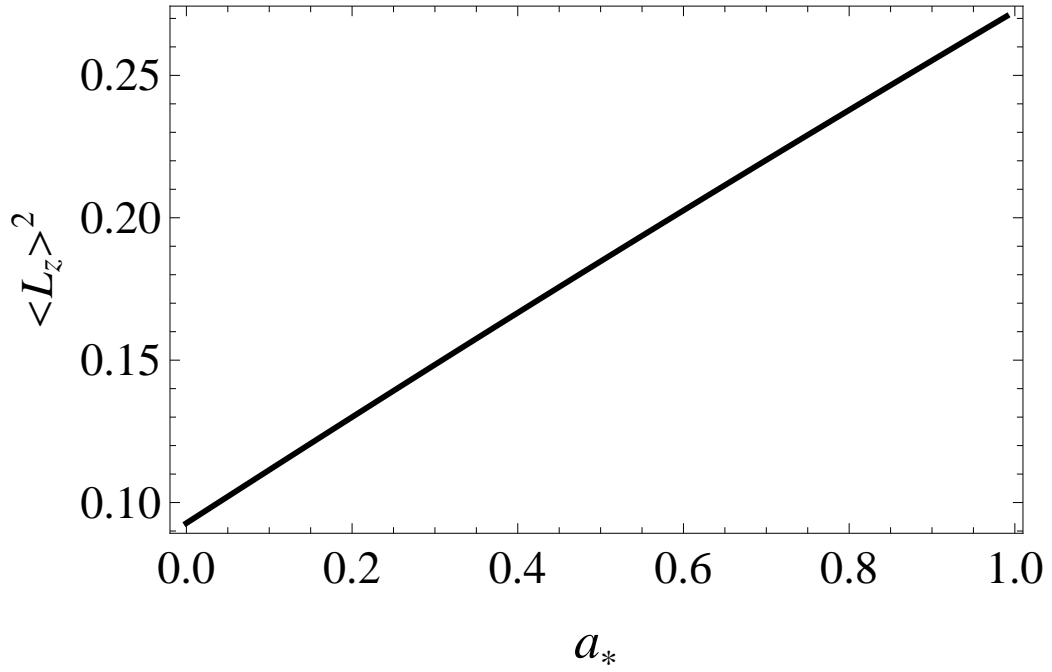


Figure 6: The dependence of $\langle L_z \rangle^2$, which is formed as the average value of L_z 's for two oppositely directed ISCOs in Kerr that share the same physical rotation rate Ω_{phys} , on a_\star is almost linear like in the Euler field. The slopes, though, are quite different.

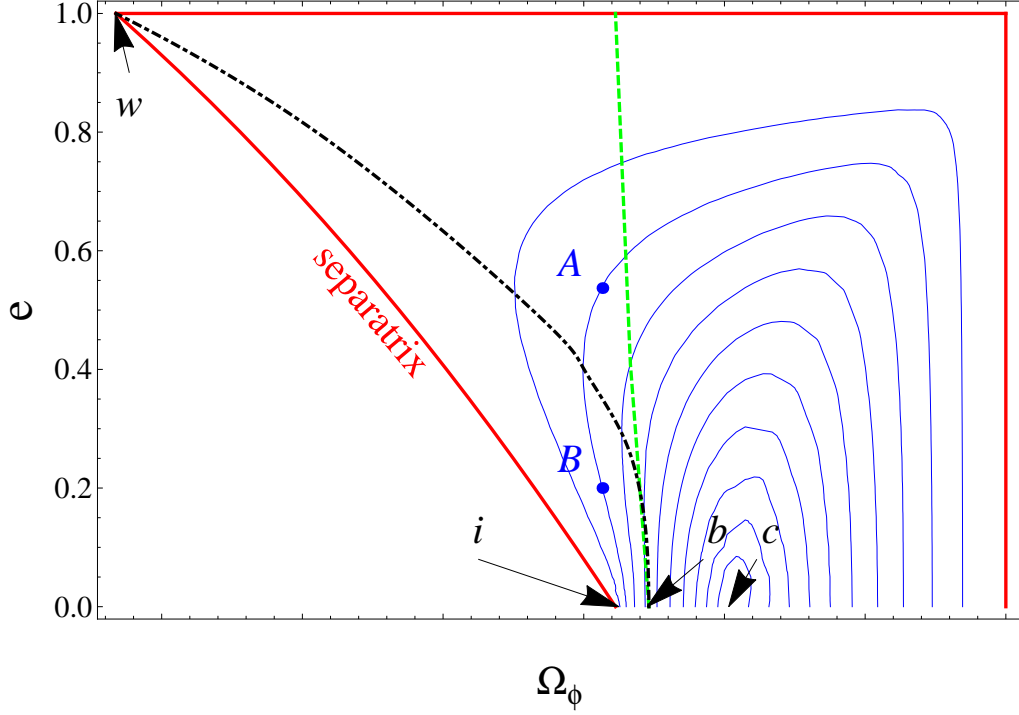


Figure 7: Contour lines of Ω_r (blue lines) for equatorial orbits in the oblate Euler potential in the $(e - \Omega_\phi)$ parameter-space (Ω_ϕ is increasing as you move towards the left in order to get a better comparison with Figure 4 of [27] and there are no numbers marked since the actual values of Ω_ϕ depend on $\sqrt{M/a^3}$). The boundary (red line) of all iso- Ω_r curves correspond to $\Omega_r = 0$, while as one move towards the smaller contours, Ω_r increases. The point along the Ω_ϕ -axis, marked ‘c’ correspond to the highest Ω_r , (see Table 1). The oblique, slightly curved part of the boundary is the separatrix, corresponding to orbits with $r_2 = r_3$, for two of the four roots r_1, r_2, r_3, r_4 of V_r potential. The corresponding orbits evolve to eternally circular orbits with radius $r = r_2$. The highest value of Ω_ϕ , marked ‘w’, corresponds to a marginally open orbit ($e \rightarrow 1$) along the separatrix. Ω_ϕ is maximized for such an orbit because as you move higher on the separatrix the double root $r_2 = r_3$ is lowered, and the orbit moves closer to the strongest part of the field. The dashed green line (the COD) is the locus of all non-circular orbits with a circular dual that is characterized by exactly the same set of frequencies (Ω_r, Ω_ϕ) . Finally the black dashed-dotted line is the singular curve along which all orbits are marginally different pairs of iso-frequency orbits. Among all pairs with the same set of frequencies that one could find on the left side of the green COD curve, we have isolated a single pair of orbits (two blue points denoted A and B) that we have thoroughly studied. Some of the contour lines, especially around point ‘c’, are not very smooth, due to inaccurate interpolation of *Mathematica* package.

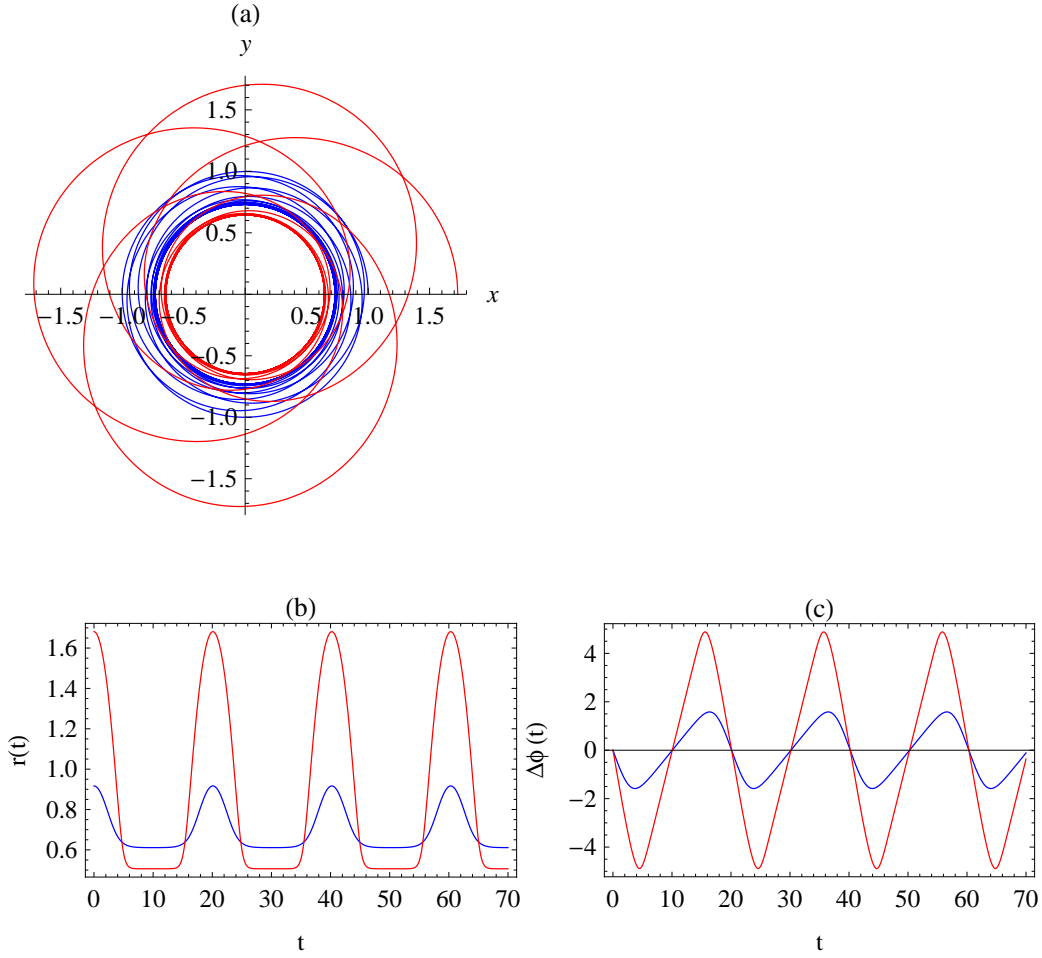


Figure 8: This plot shows the two distinct equatorial orbits A (the red more eccentric orbit) and B (the blue less eccentric one) of Figure 7 (diagram a), as well as the synchronized time evolution of their coordinates (diagrams b and c). The last diagram (c) shows the plot of $\Delta\phi(t) = \phi(t) - \Omega_\phi t$. The last two diagrams exhibit the common frequencies of the two orbits, despite the very different morphology of them.

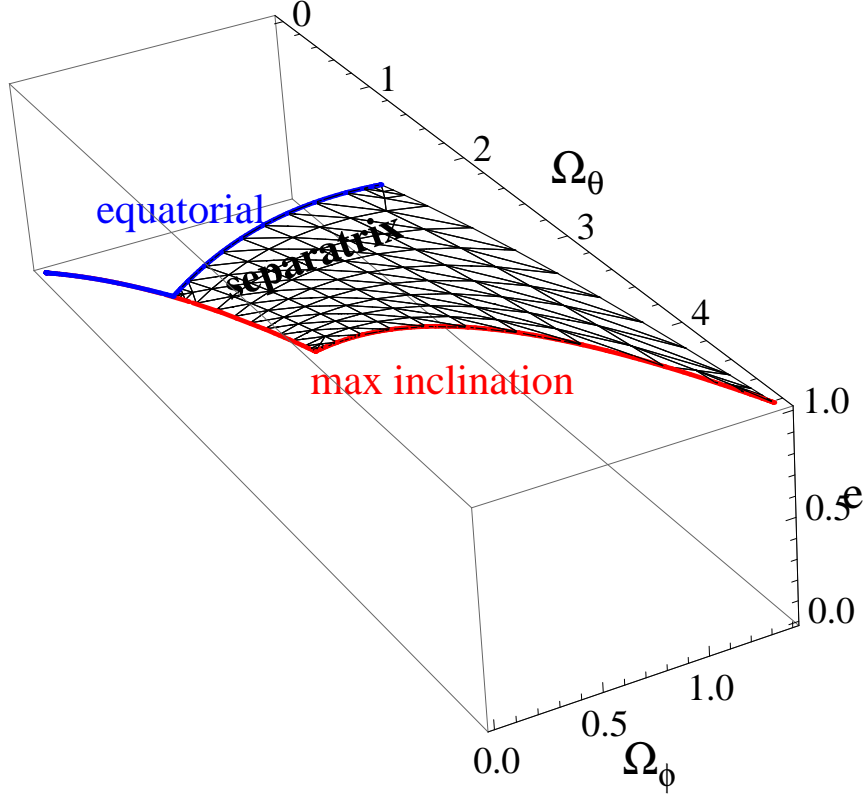


Figure 9: This plot shows two sides of the 3-dimensional parameter space $(\Omega_\phi, \Omega_\theta, e)$ of all normal bound orbits of the Euler gravitational field (one base and one of the lateral surfaces). The plot shows: (i) the separatrix strip (the grid-surface which is the locus of all orbits with $\Omega_r = 0$, apart of those with $e \rightarrow 1$ and those of infinite semi-latera recta), and (ii) the locus of spherical ($e = 0$) orbits that are either equatorial (blue solid line lying on the plane $e = 0$), or with maximum inclination (red line on the plane $e = 0$). These two lines are the boundaries of the base which are then extended along the separatrix strip, defining its boundaries (the equatorial orbits at separatrix and the most inclined orbits at separatrix). The two lines on the plane $e = 0$, are so close to each other that they look like a single curve (both are starting from the origin $(0, 0, 0)$, while the red one has a slightly greater Ω_θ frequency at a given Ω_ϕ). Furthermore, the basis of the separatrix itself is almost parallel to the maximum inclination curve on the plane $e = 0$. Thus the base of this 3-dimensional body of orbits is actually a very thin curved triangle. The same is true also with all sections of this body with the planes $e = \text{const}$ (not shown in this diagram). The full body of the orbits forms, in this parameter space, a very thin curved and skewed triangular prism, that looks more like a 2-dimensional surface. The axis of e correspond to all infinitely distant orbits that are characterized by $\Omega_r = \Omega_\theta = \Omega_\phi = 0$. A section of this body with a plane of constant Ω_ϕ , that intersects the separatrix strip has been drawn in Figure 10, along with a few iso- Ω_r contour lines.

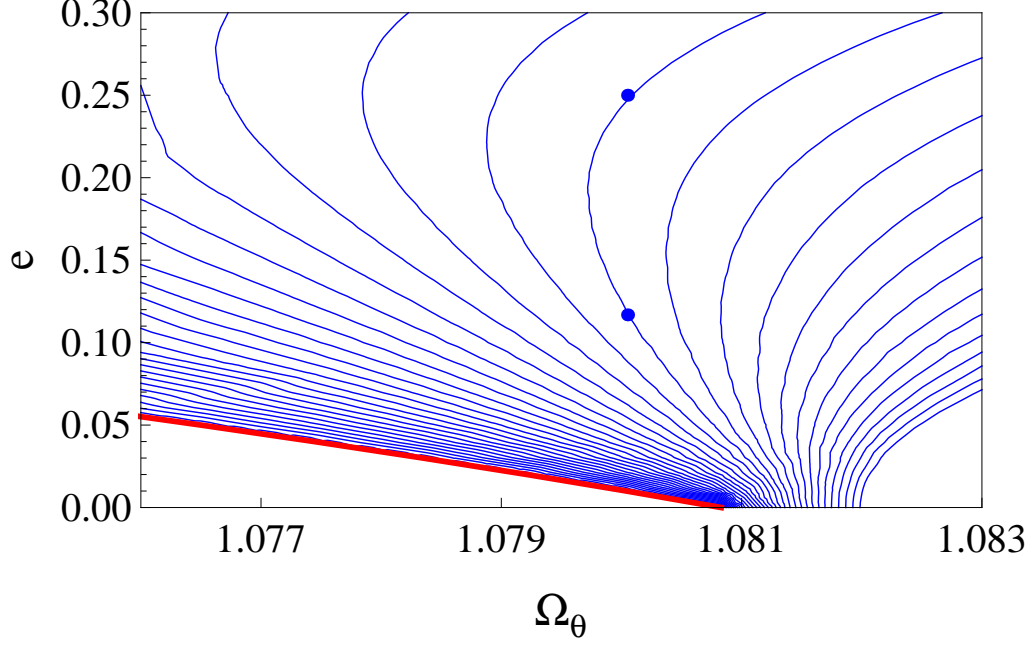


Figure 10: This is the contour plot of Ω_r in the parameter space (Ω_θ, e) of the Eulerian generic orbits, while Ω_ϕ is held fixed at a constant value, such that the plane $\Omega_\phi = \text{const}$ intersects the separatrix surface. All frequencies are expressed as multiples of $\sqrt{M/a^3}$. The segment of the parameter space depicted here is very small especially along the axis of Ω_ϕ due to the tiny width of the 3-dimensional body of orbits. It should be noted that the separatrix (the red line at the boundary of the contour plot) represents the lower values of Ω_θ . This can be easily explained from the 3-dimensional shape of the body of orbits depicted in Figure 9. In contrast, the separatrix of generic orbits of Kerr represents the higher values of Ω_θ along the section of $\Omega_\phi = \text{const}$. This is due to the different orientation of the separatrix strip in the parameter space $(\Omega_\phi, \Omega_\theta, e)$ of Kerr. A specific iso-frequency pair has been marked with two dots on the diagram. The characteristics of these two synchronized orbits are written in Table 3, while the corresponding orbits are depicted in Figure 11.

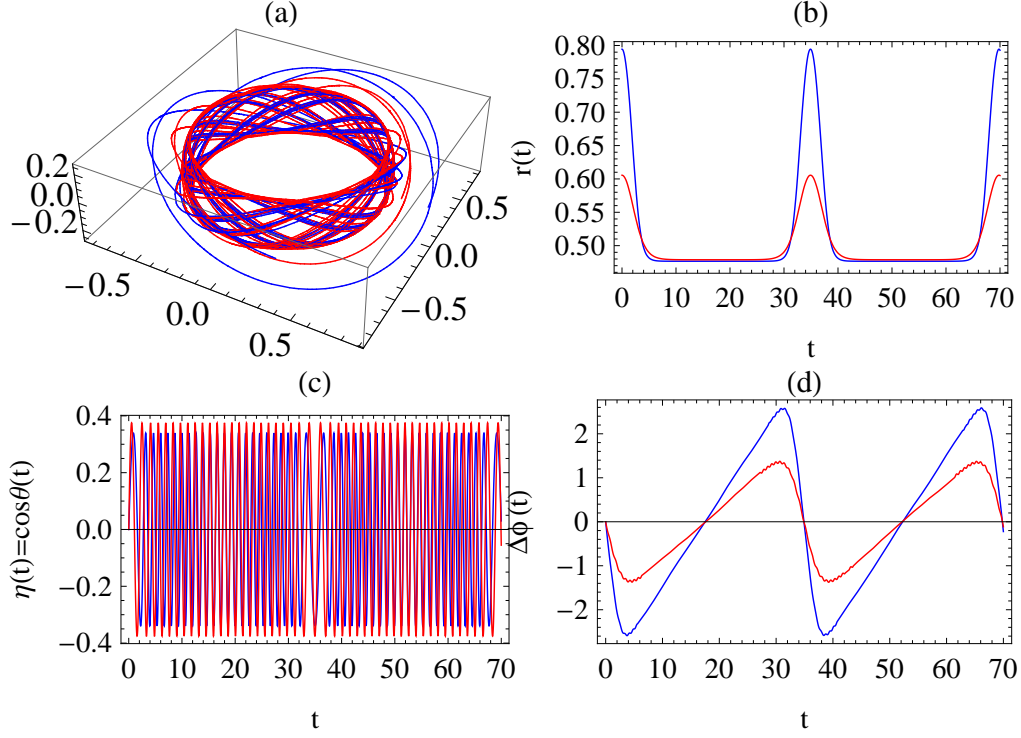


Figure 11: The specific iso-frequency pair mentioned in the previous paragraph has been plotted in this multiple figure. Diagram (a) shows the actual orbits regarding this pair (red is the orbit with the lower eccentricity, while blue is the most eccentric one). The rest three plots depict the evolution of $r(t)$, $\eta(t) = \cos(\theta(t))$, and $\Delta\phi(t) = \phi(t) - \Omega_\phi t$, respectively, for both orbits. It is clear that all three oscillations of these particular orbits are synchronized; even $\eta(t)$ in diagram (c), where there is a periodic shift between the two curves, there is no net shift when a large number of η oscillations are taken into account. The much higher value of Ω_θ (see Table 3) with respect to Ω_r is directly reflected to the corresponding plots (b and c). On the other hand the fundamental period of Ω_ϕ (which is of the same order of magnitude with that of Ω_θ) is not directly presented in plot (d), since it has been subtracted through the term $\Omega_\phi t$. The apparent periodicity of this diagram is simply a multiple of the corresponding fundamental period.

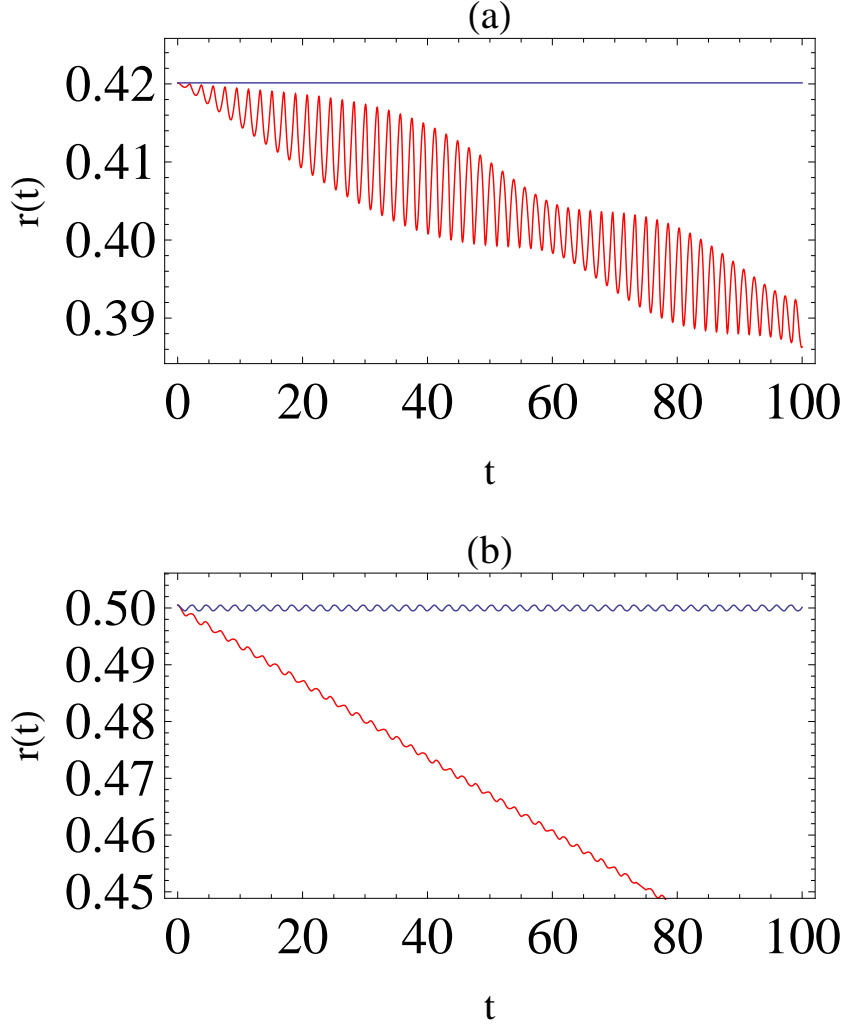


Figure 12: This plot shows the evolution of a bound Eulerian orbit under the dissipative force of Eq. (109). The evolution of the orbits have been computed with respect to normal time, t , and not with respect to Mino-type time, λ . Diagram (a) corresponds to a geodesic (when the external force is absent) circular orbit that initially is at resonance, that is, $\Omega_r(0) = 2\Omega_\theta(0)$. The blue curve shows the evolution of the radial coordinate when the external force is zero. Since the orbit is circular there is no change on $r(t)$ then. The red curve shows the evolution when the self-force is turned on. Due to resonance, radial oscillations are excited, while the orbit drifts to lower r values. Diagram (b) shows the corresponding evolution of an orbit when there is no resonance. More specifically this orbit was chosen to have initially $\Omega_r(0)/(2\Omega_\theta(0)) = 0.6$. If the self-force is absent (blue curve) the orbit oscillates slightly due to the small initial eccentricity introduced in the initial conditions. When the self-force is turned on (red curve) the radius of the orbit drifts to lower values without any apparent increase in its eccentricity. The different average slope of the two red curves is due to the fact that the initial conditions are completely different.

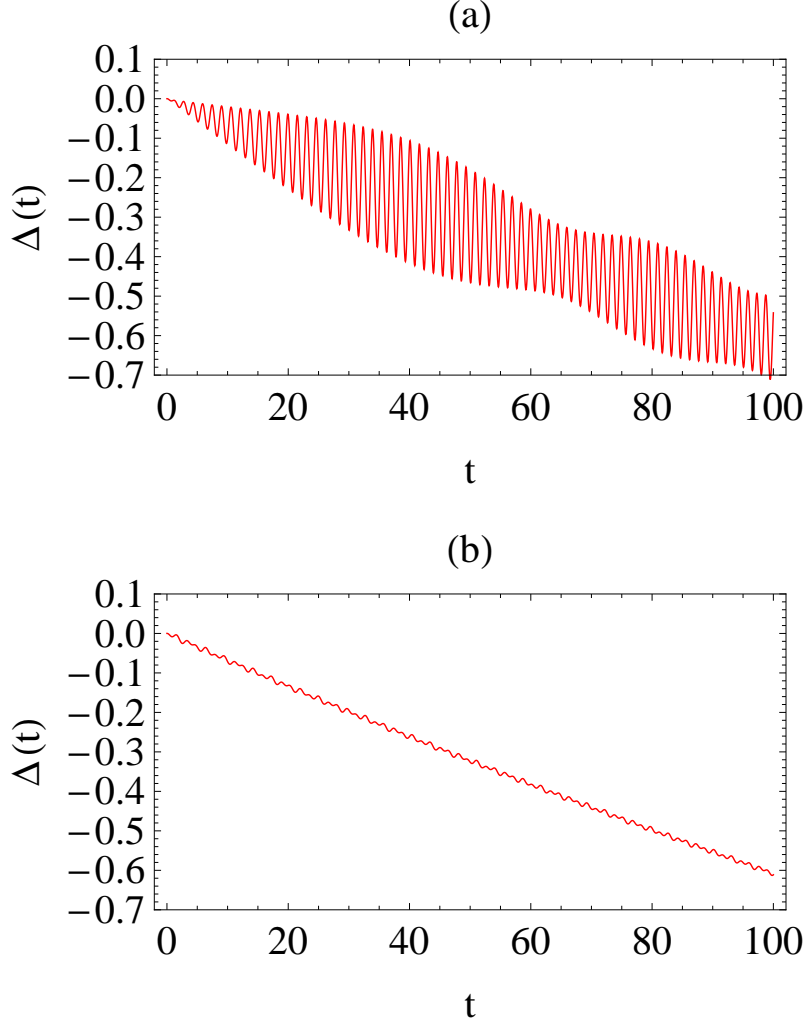


Figure 13: The two diagrams show the evolution of the driven harmonic oscillator described in Eq. (108). The frequency of the oscillatory part of the driving force is $k\omega_0$, where ω_0 is the initial frequency of the oscillator. In plot (a), $k = 1$. Thus the amplitude of the oscillator increases due to resonance. Later on the resonance condition is lost due to frequency shift and the amplitude starts decreasing. In the second plot (b), $k = 0.6$. Now there is no resonance, and the oscillator simply drifts to lower values (the e_3 term in Eq. (108) is positive) without any apparent amplitude increase.